Energy Advances

REVIEW ARTICLE

View Article Online
View Journal | View Issue

Cite this: *Energy Adv.*, 2023, 2, 1800

High entropy materials—emerging nanomaterials for electrocatalysis

Hang Li,[a] Li Ling,[b] Shengfa Li,[a] Feng Gao *[b] and Qingyi Lu *[a]

In recent years, high entropy nanomaterials (HEMs) have become a rapidly developing research field. Due to their multi-element composition and unique high entropy state, HEMs produce four typical effects (high entropy effect, sluggish diffusion, severe lattice distortion and the so-called cocktail effect) that lead to adjustable activity and enhanced stability. These HEMs have received a great deal of attention in catalyst design and exploration. However, this great potential also comes with great challenges, which is called the coexistence of opportunity and crisis. The challenges arise from their broad element composition and complex atomic arrangement configurations, which prevent the thorough and detailed study of HEMs synthesis and their inherent mechanism understanding. Due to the introduction of anions, high entropy compounds usually have more complex high configurational entropy relative to high entropy alloys, which can provide unexpected properties conducive to a wide range of applications in catalysis. Herein, we review the synthesis, structural design and electrocatalytic applications of HEMs electrocatalytic materials in recent years. Firstly, the development and the advanced characterization methods of HEMs are reviewed. Then, the superior properties of the HEMs due to their multi-element properties are discussed in different electrocatalysis applications including oxygen reduction reaction (ORR), oxygen evolution reaction (OER), hydrogen evolution reaction (HER), carbon dioxide reduction reaction (CO_2RR) and alcohol oxidation. Finally, we point out the existing challenges and propose solutions to these challenges in order to promote the development of HEMs in the field of electrocatalysis.

Received 28th June 2023,
Accepted 16th September 2023

DOI: 10.1039/d3ya00305a

rsc.li/energy-advances

1 Introduction

Scientists usually use entropy to represent a measure of the state of some material system or the extent to which some material system state is likely to occur.[1] In the field of materials science, atoms are arranged in a variety of ways, resulting in a variety and complexity of materials. This result provides a broad playground for the concepts of entropy and disorder to fulfill their functions and exhibit surprisingly interesting characteristics.[2] High entropy materials (HEMs) were first reported for metal alloys in 2004.[3,4] The emergence of HEMs immediately attracted great attention from all fields of materials chemistry, especially catalysis. The reaction pathway of catalytic reactions is fundamentally dependent on the entropy-driven behavior of the molecular species (including adsorption of the reactants, and translation, rotation, and vibration of intermediates bound to the active sites).[5] Among them, entropy contribution is an important driving force to accelerate the catalytic reaction rate by reducing activation energy.[6] By adjusting the entropy parameters of the catalyst, the stability and transformation of molecules on the catalyst can be optimized effectively under various conditions.[7] In terms of catalysts, it is very challenging to design and optimize catalysts from the perspective of entropy, especially configurational entropy, which is determined by the mixing (physical or chemical scale) of different components. This is mainly due to the diversity of configurational adjustability in multicomponent and the complexity of structure and composition that are difficult to decouple.[8–10] Recent advances in HEMs provide a multifunctional platform for studying the effects of entropy on the structure and composition of catalysts.

The basic principle of HEMs is that forming a single phase material with a high ratio of five or more main elements (equimolar or non-equimolar) will yield a high configurational formation entropy.[11] HEMs have been reported to have some unique changes over traditional polymetallic compounds, such as high entropy effect,[12] sluggish diffusion,[13] severe lattice distortion[14] and the so-called cocktail effect,[15] which all lead

[a] State Key Laboratory of Coordination Chemistry, Coordination Chemistry Institute, Collaborative Innovation Center of Advanced Microstructures, School of Chemistry and Chemical Engineering, Nanjing University, Nanjing 210023, P. R. China. E-mail: qylu@nju.edu.cn
[b] Department of Materials Science and Engineering, Jiangsu Key Laboratory of Artificial Functional Materials, Collaborative Innovation Center of Advanced Microstructures, College of Engineering and Applied Sciences, Nanjing University, Nanjing 210023, P. R. China. E-mail: fgao@nju.edu.cn

to excellent performances, such as high hardness,[16] strong corrosion resistance[17] and high catalytic activity.[18] The high entropy effect describes multiple principal elements producing a single entropy-stable phase, which may lead to the formation of high performance materials with unexpected/rare phases.[12] The sluggish diffusion effect presents that the sluggish diffusion rate makes the HEMs less prone to grain coarsening and recrystallization at high temperature, so the HEMs have good thermal stability.[13] In addition, the sluggish diffusion effect also makes it easy for HEMs to obtain supersaturated solid solutions, which is conducive to the acquisition of nanoscale precipitates. The serious lattice distortion effect is caused by the inconsistence of the atomic radius of each element in HEMs and its random distribution property, which affects the active sites of each unit, thermodynamic stability and microstructure of the synthesized HEMs crystal.[14] The ''cocktail'' effect is a phrase first used by Prof. S. Ranganathan. The original intention was ''a pleasant, pleasant mixture''. Now, it means a collaborative concoction where the end result is unpredictable and greater than the sum of its parts.[19] Unlike other core effects, the cocktail effect is not hypothetical and does not need to be proven. Cocktail effect refers to special material properties, often resulting from unexpected synergies. It is important to note that these effects are not limited to high entropy metal alloys (HEAs),[20] but also apply to other HEMs, such as high entropy metal sulfides (HESs),[18] high entropy metal nitrides (HENs),[12] high entropy metal phosphides (HEPs),[21] and high entropy metal oxides (HEOs).[1] It has been widely discussed in many recent studies.

In recent years, the synthesis and application of HEAs have been reviewed, but the entropy stabilized systems and structures of high entropy metal compounds are rarely studied. Just as the properties of traditional catalysts are closely related to composition and structure, elucidation of the structure–property relationships of HEMs, especially among different components and structures, is crucial for the use of entropy-enhanced structure–activity relationships for catalysis.[22] The rapid development of HEMs also requires a certain degree of generalization and comparison to reveal the correlation between catalyst structures and components. Here, we review the recent progress of HEMs in the field of electrochemical catalysis. This review mainly designs the following aspects: (1) we first introduce the evolution process from traditional HEAs system to entropy-stable HEMs (*e.g.*, HEPs, HEOs, HENs, HESs, *etc.*) and the corresponding preparation methods from a basic point of view. It is then summarized that a wide range of entropy-stabilized multicomponent systems with tailored components and structures can be obtained using traditional and advanced synthesis methods. (2) Advanced characterization techniques provide detailed information on the surface, electronic structure, lattice, and composition of HEMs, which are important for understanding the related catalytic behaviors. (3) Then, case studies of HEAs and high-entropy compounds are carried out, highlighting the links between structure, component, and electronic properties and the catalytic properties. (4) Finally, we discuss the upcoming opportunities and challenges for HEMs. We hope that the insights provided here will contribute to the future design and development of HEMs with high performance, diversity of structure or components.

2 Synthesis of HEMs

HEMs are developed from multicomponent alloy systems. Therefore, the initial reports of HEMs were presented through alloy systems with more components.[3,4] At the same time, HEMs also inherit some typical characteristics of alloyed materials. The different atoms of HEMs are randomly distributed in an ordered manner. HEMs have unique and favorable physical and chemical properties due to the interaction of more elements.[23] This unique structure not only improves the efficiency of atomic utilization, but also promotes a more catalytic electronic structure.[24] This has been demonstrated in many cases, such as the application of the four effects of HEMs in various fields described in the introduction. Their unique physical and chemical properties are due to the uniform dispersion of components and structural adjustability caused by the single-phase structure of alloy-like materials.[25] Construction of the active interface domain also requires fine control, as the formation of impurities prevents surface exposure of the active site.[26] Therefore, maintaining a single-phase state is essential to achieve atomic mixing of different components and to obtain the synergistic properties.[27]

In order to achieve this goal, many researchers have proposed different methods to prepare HEMs with single-phase structure. HEMs were first reported by Yeh *et al.* in 2004, this work is an extraordinary realization of multiple elements ($CuCoNiCrAl_xFe$) co-existing in a single phase by an arc melting method (Fig. 1a).[3] Arc melting is a method of electrothermal metallurgy in which electric energy is used to produce an arc between electrodes or between electrodes and materials to be melted.[28] Subsequently, Chang *et al.* followed and reported a composition-adjustable six-element $Fe_{16.7}Cr_{16.7}Mn_{16.7}Ni_{16.7}Co_{16.7}M_{16.7}$ (M = Nb, Ge, Cu, Ti and V) single-phase alloy materials by casting and melt spinning, in which the six elements have an equal molar ratio. The basic principle of this method is based on heating to melt the raw material into a certain viscosity melt, and finally form a homogeneous solid solution material.[4] These two works are recognized as prototypes of HEMs, and HEMs gradually stepped into the materials field.

Soon afterwards a nanoparticle with adjustable composition and layered distribution of elements (Au, Ag, Cu, Ni and Co) was synthesized by a novel technique (scanning-probe block copolymer lithography) in 2016 (without uniformly elemental dispersion in the end). The basic principle of the method is that an atoliter-scale volumes of polymers with a metal ion precursor to the desired location on the surface can form as a nanoreactor to convert the precursor into a single site-isolated nanoparticles (NPs) after heat treatment. This work enables the controlled preparation of five different metal components in individual nanoparticle. The researchers extend the element

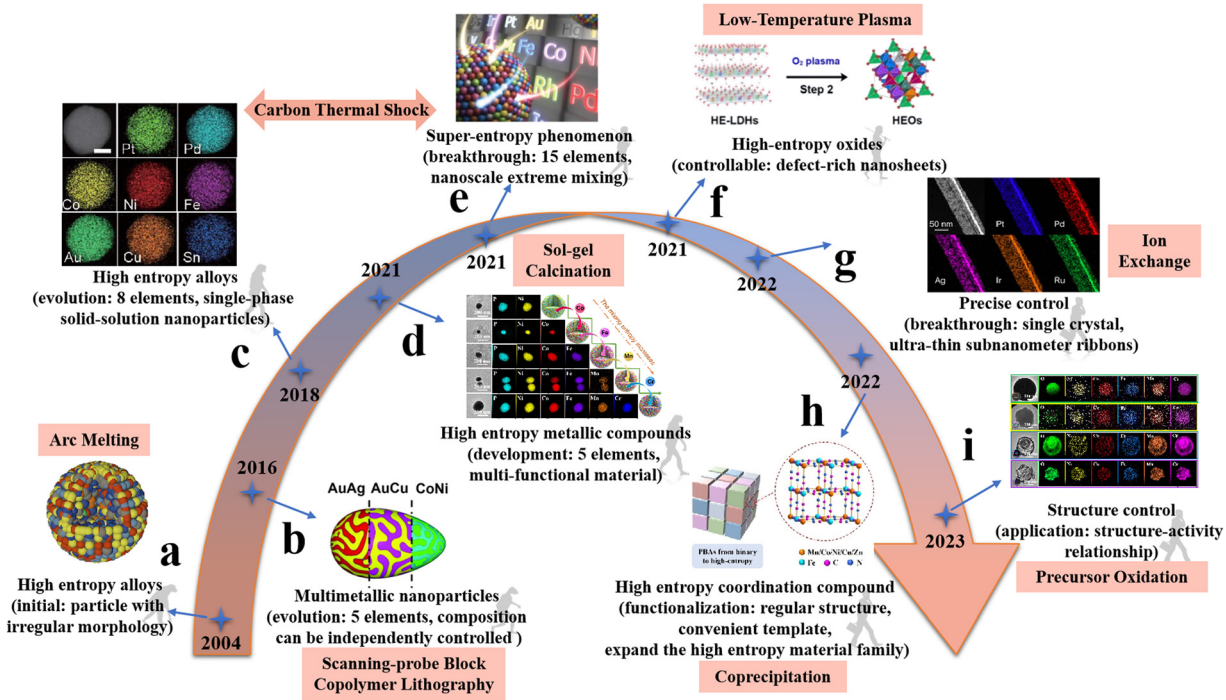

Fig. 1 Development and evolution of high-entropy materials with varying morphology and adjustable composition through different synthesis strategies. (a) Bulk high entropy alloys ($CuCoNiCrAl_xFe$). Reprinted with permission.[3] Copyright 2004 Wiley-VCH. (b) A nanoparticle with adjustable composition and layered distribution of elements was synthesized (without uniformly dispersive elements in the end). Reprinted with permission.[30] Copyright 2016 AAAS. (c) Multicomponent NPs (PtPdCoNiFeCuAuSn). Reprinted with permission.[31] Copyright 2018 AAAS. (d) High-entropy metal phosphide (NiCoFeMnCrP). Reprinted with permission.[32] Copyright 2021, The Royal Society of Chemistry. (e) HEAs with 15 elements by using carbon thermal shock technology and fast moving bed pyrolysis technique. Reprinted with permission.[33] Copyright 2021, Elsevier Ltd. (f) HEOs nanosheets ($(FeCrCoNiCu)_3O_4$). Reprinted with permission.[34] Copyright 2021, Wiley-VCH. (g) Ultra-thin two-dimensional HEA subnanoribbons (SNRs) composed of up to eight metal elements (PtPdIrRuAg). Reprinted with permission.[35] Copyright 2022, American Chemical Society. (h) High-entropy Prussian blue materials. Reprinted with permission.[36] Copyright 2022, Wiley-VCH. (i) HEOs (CrMnFeCoNiO). Reprinted with permission.[37] Copyright 2023, The Royal Society of Chemistry.

composition to noble and transition metals (Fig. 1b).[29] Then Hu *et al.*[30] synthesized a wide range of multicomponent NPs (PtPdCoNiFeCuAuSn) with a desired chemistry (composition), size, and phase (solid solution, phase-separated) by controlling the carbothermal shock (CTS) parameters (substrate, temperature, shock duration, and heating/cooling rate). In this method, NPs can be generated by simply loading a metal precursor onto a carbon substrate and running a short current through the sample to raise the temperature instantaneously (Fig. 1c). In 2021, HEMs are like bamboo shoots after a spring rain, more and more researchers are committed to the development and research of HEMs. Lai *et al.* prepared a gel containing five kinds of metal species (Fe, Co, Ni, Cr and Mn) and phosphorous species by sol–gel method, and successfully realized the preparation of HEPs after calcining the obtained gel precursor at high temperature (Fig. 1d).[31] Hu *et al.* made a breakthrough in the preparation of HEAs with 15 elements by using carbon thermal shock technology and fast moving bed pyrolysis technique, which showed a solid solution structure with local strain and lattice distortion caused by extreme mixing (Fig. 1e).[32]

With the development of HEMs, researchers are no longer satisfied with the component regulation of HEMs, and more and more people pay attention to the morphological and structural regulation of HEMs. Wang *et al.* reported a low-temperature plasma strategy towards the synthesis of HEOs nanosheets with rich oxygen vacancies. Compared with the traditional high-temperature calcination/reduction method, the low-temperature plasma has the advantages of operation at room temperature, non-equilibrium property and low power, which can solve the problems of grain aggregation, sublimation and structure collapse in the traditional preparation processes, and realize the unconventional preparation of materials (Fig. 1f).[33] Guo *et al.* developed a new cryogenically general synthesis method (ion exchange method) to prepare ultra-thin HEA subnanoribbons (SNRs) composed of up to eight metal elements with a layer thickness of only 0.8 nm, achieving the thinnest HEA metal material in the world, using Ag nanowires (NWs) as a template (Fig. 1g).[34] Du *et al.* expanded the family of HEMs and successfully prepared high-entropy Prussian blue materials with cubic morphology by simple coprecipitation method (Fig. 1h).[35] Recently, our research group proposed a universal precursor oxidation method to simultaneously achieve the synthesis and structure regulation of HEOs.[36] Different metal sources are uniformly integrated into amorphous carbon spheres through a hydrothermal process. The resulted carbon spherical precursor are transformed to crystalline HEMOs after an oxidation

process and by controlling ion diffusion and oxidation rates, HEMOs with different structures including solid, core–shell and hollow spheres can be controllably achieved.

3 Characterization of HEMs

High entropy NPs should be a single-phase structure, showing a homogeneous and random mixture of constituent elements.[37] However, describing this random mix of multiple elements and their synergies is very challenging. At present, it is necessary to develop more advanced characterization techniques in addition to conventional characterization techniques in order to systematically understand the structure and component characteristics of HEMs. Here we provide an overview of commonly used diffraction, microscopy, spectroscopy and more advanced characterization techniques (Fig. 2a).

Powder X-ray diffraction (XRD) can help determine the basic phase structure to make sure whether the material is homogeneous.[38] Electron-coupled plasma atomic emission spectrometry (ICP-AES) can accurately determine the molar ratio of each metal element in HEMs,[39] and X-ray photoelectron spectroscopy (XPS) can help determine the valence states of basic elements.[40] XPS not only provides information about molecular structure and valence states for chemical research, but also provides information about elemental composition and content, chemical state, molecular structure and chemical bond of various compounds. But these characterization techniques may lack the resolution needed to analyze the more elemental mixing. Synchrotron X-ray technology has been widely used in materials research, mainly because the technology can provide shorter wavelengths, which can better characterize the atomic arrangement, bonding coordination and electronic properties of HEMs.[41] For example, synchrotron XRD has high resolution and diffraction intensity and is suitable for studying long range and/or short range ordered crystal and amorphous materials.[42] Therefore, synchrotron XRD can more accurately detect the overall phase structure and possible immiscible phase and impurities in HEMs. X-ray intensity attenuates after passing through the sample, and the degree of attenuation is closely related to the structure and composition of the sample. This study of the relationship between transmission intensity and incident X-ray intensity is called X-ray absorption spectroscopy (XAS).[43] Because its transmitted

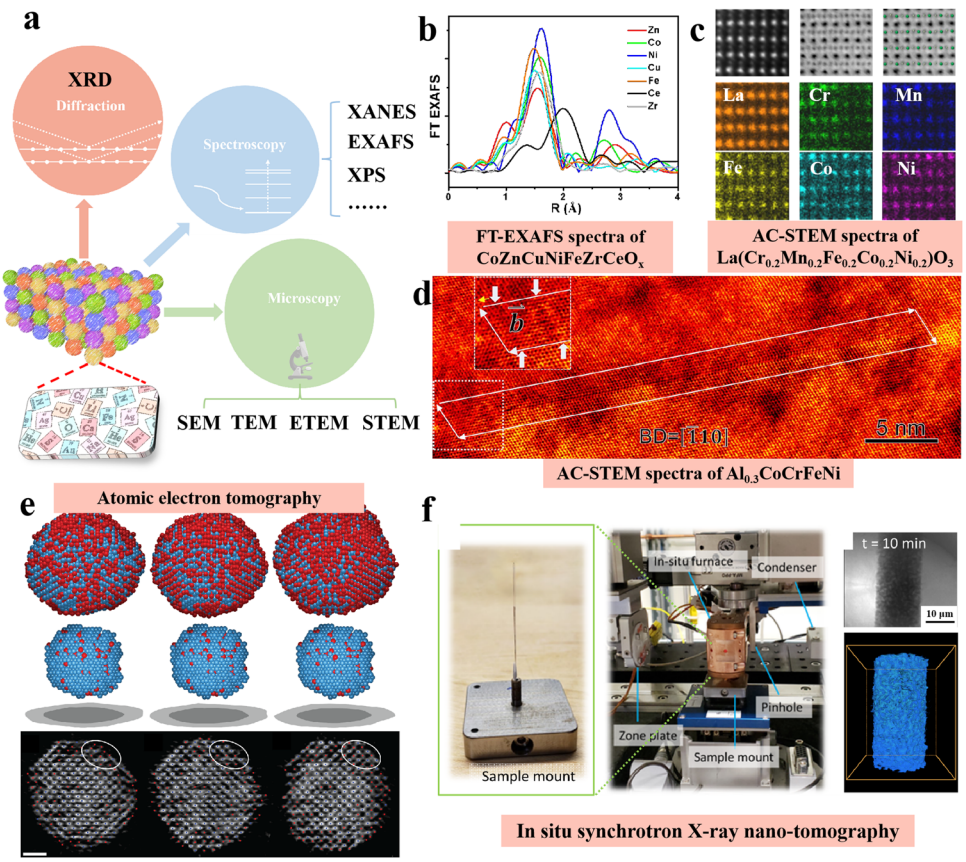

Fig. 2 Advanced characterization techniques for high-entropy materials: (a) schematic summarizing the diffraction, microscopy, and spectroscopy techniques for the characterization of HEMs. (b) FT-EXAFS spectra of CoZnCuNiFeZrCeO$_x$. Reprinted with permission.[53] Copyright 2018, American Chemical Society. (c) HAADF-STEM, ABF and atomic EDS mapping of La(Cr$_{0.2}$Mn$_{0.2}$Fe$_{0.2}$Co$_{0.2}$Ni$_{0.2}$)O$_3$. Reprinted with permission.[54] Copyright 2022 Springer Nature. (d) AC-HAADF-STEM image of Al$_{0.3}$CoCrFeNi. Reprinted with permission.[55] Copyright 2018, Elsevier Ltd. (e) Atomic electron tomography. Reprinted with permission.[56] Copyright 2019, Springer Nature. (f) *In situ* synchrotron X-ray nano-tomography. Reprinted with permission.[57] Copyright 2021, Springer Nature.

light intensity is related to atomic number and atomic mass, for solid (crystal or amorphous), liquid, gas and other types of samples it can be used for qualitative and quantitative analysis of relevant test elements. Thus, XAS can be used to study the atomic and/or local coordination environment of each element, which is critical for understanding multi-element mixing and possible short-range or local ordering in HEMs.[44]

So far, the detection techniques of material structure are generally based on the diffraction phenomenon of crystalline ordered structures, and XAFS (X-Ray absorption fine structure spectrum) is an exception.[45] XAFS includes both XANES (X-ray absorption near edge structure)[46] and EXAFS (extended X-ray absorption fine structure)[47] technologies. In the X-ray absorption spectrum, the low-energy spectrum above the threshold within 60 eV shows strong absorption characteristics, which is called XANES.[48] It is caused by the multiple scattering of excited photoelectrons by surrounding atoms. It not only reflects the geometric configuration of atoms in the surroundings of absorbing atoms, but also reflects the structure of electron states in the low energy near the Fermi level, so it becomes a useful tool for studying HEMs. As a powerful tool to study and characterize catalysts, XANES can determine valence states, characterize D-band properties, measure coordination charges, and provide structural information including orbital hybridization, coordination number and symmetry.[49] With the development of synchrotron radiation source, the application of XANES in the study of HEMs has increased significantly. EXAFS is the oscillation of the X-ray absorption coefficient of the element in the range of 30–1000 eV on the high-energy side of the absorption edge.[50] The production of EXAFS is related to the scattering of absorbing atoms and other atoms around them, that is, they are all structure-dependent. Therefore, the nearest neighbor structure around the absorption atoms can be studied by EXAFS, and the parameters such as atomic spacing, coordination number and mean azimuth shift can be obtained.[51] The main feature of EXAFS method is that it can measure different kinds of atoms respectively, give the nearest neighbor structure of the specified element, and distinguish the types of the nearest neighbor atom. It is also possible to use strong X-ray sources to study the neighboring structures of atoms in very small quantities, and to study both ordered and disordered matter. In this way, EXAFS can be used to solve structural problems that are difficult or impossible to solve with other methods.[52] As shown in Fig. 2b, Liu *et al.* proved that there are certain differences among the elements Co, Zn, Cu, Ni, Fe, Zr, and Ce in HEMs through FT-EXAFS spectra and EXAFS.[53] There are obvious differences in the relative strength, coordination number and bond distance of each metal element in the FT-EXAFS curves, which reveal the different local structure and chemical environment of each element.

Advanced electron microscopy technology is needed to better understand the particle size, morphology and distribution of each element of HEMs. Electron microscopy mainly includes scanning electron microscopy (SEM),[58] transmission electron microscopy (TEM)[59] and scanning transmission electron microscopy (STEM),[60] which rely on the interaction between electrons and samples and are widely used to obtain local information such as the morphology and size of materials. SEM has the features of large depth of field, high resolution, intuitive imaging, strong stereo sense, wide magnification range, and the sample to be tested can rotate and tilt in three-dimensional space. In addition, it has the advantages of rich sample types, almost no damage or contamination of the original sample, and the morphology, structure, composition and crystallographic information can be obtained at the same time On the other hand, STEM has a broader function. STEM enables the characterization and analysis of the microstructure and fine chemical components of materials at the nano and atomic scale.[61] In recent years, with the introduction of spherical correction, the spatial resolution of STEM has reached the level of sub-angstrom, and the imaging observation of a single atomic column can be realized. As show Fig. 2c, Su *et al.* displays the HAADF image and EDS maps of La(CrMnFeCo-$Ni_{0.2}$)O_3, respectively, confirming its chemical compositions. EDS maps show that La is uniformly distributed on the A-site, and the five transition-metal cations, namely Fe, Mn, Cr, Ni, and Co, are in the B-site. Oxygen is observed in the ABF image, distributed between two neighboring B-site atoms. From the EDS maps the intensity variations of the five B-site TM cations can be clearly observed.[53] Xu *et al.* clearly demonstrated the dissociated $(a/2)\langle 110\rangle$ dislocation taken along the [110] direction through HAADF-STEM characterization (Fig. 2d).[54] Annular dark field STEM (ADF-STEM) allows atomic resolution visualization of HEMs that explicitly determine the positions of different atoms.[62] Elemental diagrams of STEM combined with energy dispersive X-ray spectroscopy (EDS)[63] or electron energy loss spectroscopy (EELS)[64] can specify the local chemical composition, which is important for evaluating the structural uniformity of HEMs. STEM-EDS elemental maps are more commonly applied to HEMs because of their high sensitivity to metallic elements with higher atomic numbers. EELS are able to identify the oxidation state of the target element and more sensitive detect light elements such as C, N and O. TEM is usually more focused on smaller areas with higher resolution.

In addition to the characterization techniques mentioned above, various simulation methods and calculation methods have also been applied to study the structure, composition and active site of HEMs.[65] In order to better understand the structure and atom-related information of HEMs, researchers are trying to find more advanced representations to explore the deeper structural information of HEMs. Atomic electron tomography (AET) is a powerful method for determining the three-dimensional (3D) atomic structure of materials without assuming the degree of crystallization, and has been applied to the study of dislocation, stratification, grain boundaries, atomic displacement, strain tensors, chemical order/disorder, and point defects in unprecedented details.[66] Miao *et al.*[56] reported a four-dimension (including time) study of early nucleation using atomic electron tomography (AET). Using iron base alloy NPs as a model system, the researchers found that the early nuclei were formed irregularly. Each core was composed of one to several atoms with maximum order parameter, and the order

parameter varied gradiently from the core to the edge of nucleation. The structural and dynamical changes of early nucleation during growth, decomposition and fusion were also captured, and it was found that these processes were regulated by the distribution and gradient changes of order parameters (Fig. 2e). This technique provides a new angle for studying the fundamental issues of materials science. The real-time change of material structure can help us to understand more clearly the internal structure formation mechanism of the material itself. Ronne *et al.* reported a novel characterization technique (*in situ* synchrotron X-ray nano-tomography) for the real-time detection of unique physicochemical properties and unique morphological evolution of nanomaterials (Fig. 2f).[57]

In addition to experimental characterizations, various computational methods have been applied to predict the synthesis of HEMs and to interpret the catalytic behavior of HEMs. Density functional theory (DFT) calculations can evaluate atomic configuration, electron distribution and energy parameters of HEMs.[67] The birth of artificial intelligence has a great impact on the field of material synthesis. The derived machine learning technique can achieve high throughput screening of possible structures and compositions in HEMs.[8] The advent of this technology has greatly accelerated the process of material discovery and design. In addition, based on computer simulation techniques, researchers used molecular dynamics and Monte Carlo methods to achieve controllable prediction of the composability and stability of HEMs.[68] With the innovation of artificial intelligence and computer technology, these computational tools can not only produce results that complement experimental data, but also guide the progress of experiments.

4 HEMs for electrocatalysis

Electrocatalysis is a kind of catalysis that accelerates the charge transfer at the interface of electrode and electrolyte. The range of electrode catalysts is limited to electrode materials such as metals and semiconductors.[69] Under the background of The Times, electrocatalysis applications are playing an increasingly important role in sustainable and clean energy conversion.[70] The unique structure and four effects of HEMs make it more suitable for application in the field of electrocatalysis. The significant advantages of multi-cationic methods have been demonstrated by studies of low entropy binary and ternary catalysts.[71] Therefore, many researchers have carried out systematic experimental and theoretical studies using HEMs to achieve efficient and controllable electrochemical transformation of small molecules such as H_2O,[72] O_2,[73] CO_2[74] and C_2H_5OH.[75] The rise of HEMs has revolutionized the field of electrocatalysis in terms of performance. The research on the electrocatalysis performance of HEMs has also gradually developed from the initial performance improvement to the structure–activity relationship. In other words, recently more and more researchers are paying attention to the bidirectional controllable constructibility of HEMs' components and morphology. We believe that the development of HEMs is bound to go through the difficult road of element composition harmonization and morphology control. On the one hand, it is due to the consideration of different electrocatalytic environments, so that HEMs can better adapt to various application environments. On the other hand, this is the pursuit of the majority of material chemists, because it is not difficult to design a theoretical optimal architecture, the difficulty is to design a "just right" architecture under various conditions. Therefore, next, we will focus on some HEMs electrocatalysis work with morphology and structure regulation, in order to provide some useful information for readers interested in this field.

4.1 Oxygen reduction reaction

Oxygen reduction reaction (ORR) is one of the indispensable half-reactions essential in new energy storage and conversion systems such as fuel cells and metal air batteries.[76] However, ORR's multi-step and slow electron transport and low mass transfer efficiency result in its slow kinetic speed, which greatly hinders its application in practical devices.[77] Therefore, it is necessary to develop highly efficient ORR catalysts that can achieve both rapid charge transfer and mass transfer. At present, Pt-based catalysts are mainly used as electrocatalysts for ORR.[78] However, Pt is a rare metal, and its resistance to toxicity is poor resulting in non-ideal stability. The internal synergistic effect between HEMs elements can regulate the electronic state, which may improve the ORR's catalytic activity of HEMs. At the same time, the high entropy and slow diffusion effect of HEMs greatly enhance its thermal and chemical stability as well as corrosion resistance, ensuring the stable operation of HEMs under harsh conditions.[79] Previously, we have described the unique physical and chemical properties of HEMs, which also implies that it can shine in ORR. At present, more and more researchers pay attention to the influence of shape control of HEMs on catalytic performance. Chen *et al.*[80] presented a convex cubic $Pt_{34}Fe_5Ni_{20}Cu_{31}Mo_9Ru$ HEA catalyst with abundant (310) crystal faces and 38.5 nm crystal size synthesized by one-pot method (Fig. 3a). In this work, the controllable preparation of HEA with high index facets exposed were achieved through selective crystal growth, which made the prepared catalyst show excellent catalytic performance in ORR. $Pt_{34}Fe_5Ni_{20}Cu_{31}Mo_9Ru$ exhibits a half-wave potential of 0.87 V, limiting current density (j_{max}) of 5.6 mA cm^{-2} and Tafel slope of 69 mV dec^{-1}. The current density of HEA catalyst remains 89% after 40 h, exhibiting outstanding long-term stability. However, overly complex models may make it difficult to study the structure–activity relationship of HEAs. The preparation of high-index facets nanocrystals and the relationship between the shape and structure of nano-HEAs and their catalytic properties have not been thoroughly studied.

Synthesis of heterogeneous catalysts is one of the important strategies to improve catalytic performance. Bueno *et al.*[81] reported the synthesis of quinary higher order HEAs (PdCuPtNiM, M = Co, Ir, Rh, Fe, Ru and Rh) through thermal conversion of core@shell NPs. Core@shell HEA NPs were prepared by the seed-mediated co-reduction. And then, the NPs were dispersed on carbon support and annealed to promote the mixing

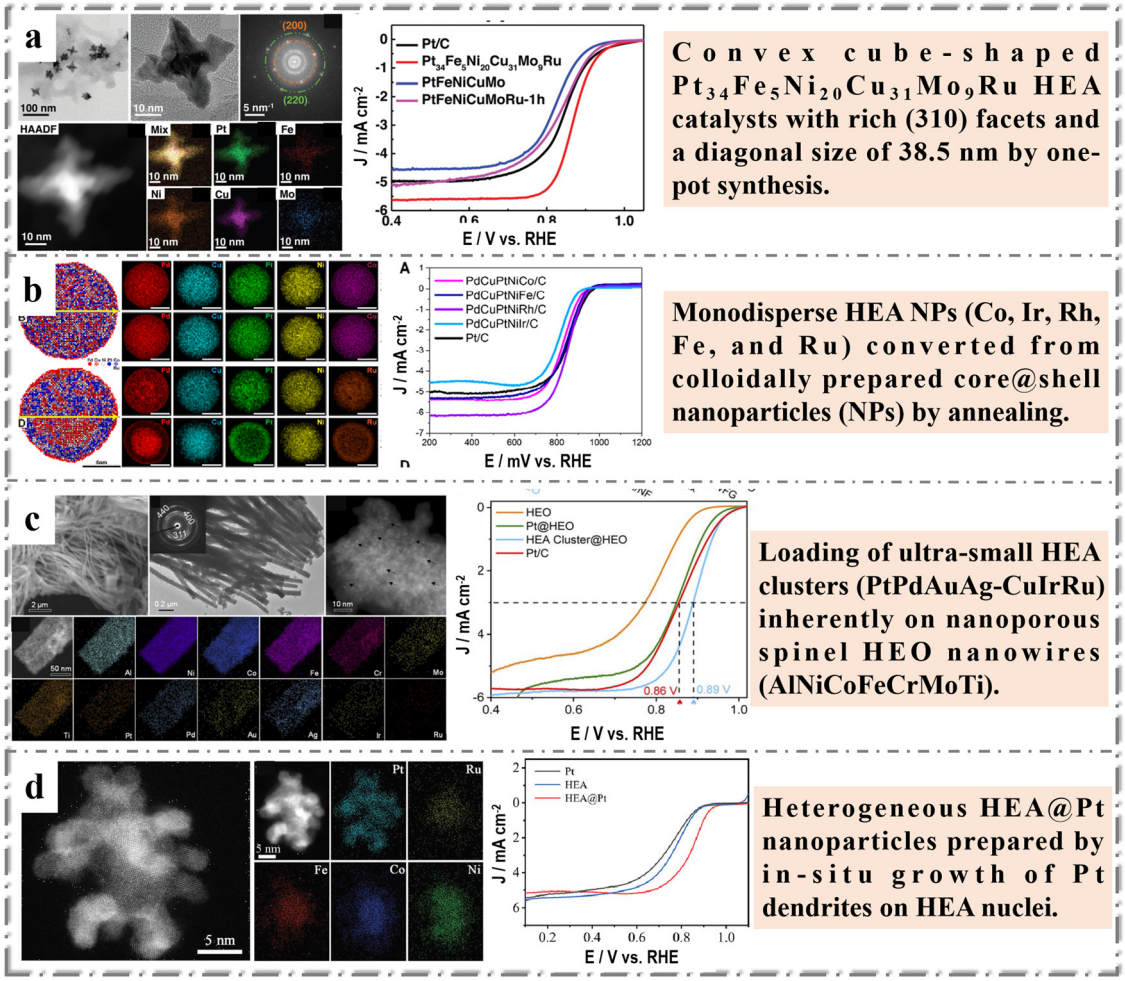

Fig. 3 Examples of HEMs in ORR: (a) Convex cube-shaped $Pt_{34}Fe_5Ni_{20}Cu_{31}Mo_9Ru$ HEA catalysts: high angle annular dark field TEM image and the corresponding elemental mapping of $Pt_{34}Fe_5Ni_{20}Cu_{31}Mo_9Ru$ and electrocatalytic performance of samples (polarization curves). Reprinted with permission.[80] Copyright 2022, Wiley-VCH. (b) PdCuPtNiRu core@shell NPs: atomistic simulations of the phase stability of the quinary HEA NPs, electrocatalytic performance of samples (polarization curves). Reprinted with permission.[81] Copyright 2022, American Chemical Society. (c) Fourteen-component high-entropy alloy@oxide electrocatalyst: characterization (SEM, TEM, HAADF-STEM and STEM-EDS mapping) of the HEA cluster@HEO and electrocatalytic performance of samples. Reprinted with permission.[25] Copyright 2022, The Royal Society of Chemistry. (d) HEAs spatial heterostructure electrocatalyst: structural characterizations (HAADF STEM image and EDS mapping images of HEA@Pt) and electrocatalytic performance for ORR. Reprinted with permission.[82] Copyright 2023, Wiley-VCH.

and formation of single-phase PdCuPtNiCo NPs. For NPs containing Ir and Ru, intra-particle heterogeneity, *i.e.*, subdomains within a single NPs with different metal distributions, was observed. The resulted core@shell HEA NPs show better activity and durability than commercial Pt (Fig. 3b). In this work, the electron controllable modulation and the adsorption energy optimization of the active site for intermediates of HEA materials were realized based on the heterostructural regulation of HEA.

In order to further adjust catalytic performance and versatility, the design and manufacture of multi-component high entropy nanocomposites such as HEA@HEO should be very promising. Jin *et al.*[25] designed a two-step alloy-dealloying strategy to synthesize ultra-small HEA nanoclusters (~2 nm) loaded on nanoporous HEO nanowire, and realized the composition of HEA and HEO that could be individually controllable adjusted. The combined experimental results and first-principles DFT calculations clearly show that better oxygen evolution (OER) performance can be obtained by optimizing the composition of HEO carriers, and that, compared with pure Pt clusters, due to the modified optimized surface electronic structure, the seven-component HEA nanoclusters show more excellent catalytic activity for ORR (Fig. 3c). However, we believe that another unique advantage of HEAs is the adjustable proportion distribution of each element, which may greatly increase the catalytic activity of HEAs. Recently, Zhang *et al.*[82] reported an effective strategy to accelerate the ORR/OER dynamics of Li–O_2 batteries by constructing a unique, well-designed HEAs spatial heterogeneous electrocatalyst (HEA@Pt) as a cathode. The core–satellite structure promotes the rapid transfer of interfacial electrons and exposes active heterogeneous interfaces for catalytic reactions, thus increasing the intrinsic catalytic activity of ORR (Fig. 3d).

4.2 Oxygen evolution reaction

OER is a four-electron–proton coupling reaction. Its mechanism is very complex resulting in the slow reaction kinetics, so the overpotential (potential difference between the electrode potential and the equeilibrium potential (1.23 *V vs.* RHE)) is high, which is the key factor limiting the efficiency of water electrolysis. The design and synthesis of high efficiency OER catalyst is the key to improve the efficiency of hydroelectrolysis. Currently, the most effective OER catalysts are the oxides of the precious metals iridium and ruthenium (IrO_2 and RuO_2, *etc.*), but their scarcity severely limit their large-scale application.[83] Recent studies have shown that electrocatalysts designed from alloys of two or more elements (*e.g.*, transition metals, TM) show promising enhancements in catalytic activity and durability due to synergistic effects of the alloys, such as strain engineering or valence electron exchange.[84] The high positive potential required by OER tends to oxidize the surface of the metal catalyst and form metal oxides or (oxygen) hydroxides.[85] Recently, a number of HEMs with significant OER activity have been reported, such as high entropy perovskite,[86] high entropy spinel,[87] high entropy layered structure type materials,[88] HESs[89] and so on. Lai *et al.*[31] proposed the synthesis of single-phase metal phosphide NPs (including NiP, NiCoP, NiCoFeP, NiCoFeMnP and NiCoFeMnCrP) based on sol–gel method and calcination reduction strategy. It was found that with the addition of Co, Fe and Mn to form binary NiCoP, ternary NiCoFeP and quaternary NiCoFeMnP, the overpotentials can be continually decreased from 451 mV to 348 mV, 335 mV and 325 mV, respectively, which are close to that of commercial IrO_2. Further addition of Cr to form the high-entropy NiCoFeMnCrP NPs provides an excellent OER electrocatalyst with an overpotential of only 270 mV. The results also confirm that the high entropy effect and cocktail effect of HEMs significantly improve the catalytic activity of the materials. This work provides a simple and feasible synthesis strategy for the preparation of HEMs and has great potential applications in energy and electrocatalysis (Fig. 4a).

Similarly, high entropy sulfides and high entropy oxides have also been reported for OER, both exhibiting excellent catalytic properties (Fig. 4b and c). Abdelhafiz *et al.* reported *in situ* synthesis of non-noble metal HEO catalysts on carbon fiber by rapid Joule heating and quenching.[90] Compared with the noble metal IrO_2, the different compositions of three- to six-membered (FeNiCoCrMnV) HEO NPs are more active catalysts for oxygen evolution. Alloying elements Cr, Mn and V affect OER activity by promoting different oxidation states of the catalytic activity TM (Fe, Ni and Co). The introduction of more metal elements resulted in the serious distortion of crystal structure, which may be the reason for the excellent catalytic performance of HEMs. Cui *et al.*[91] first reported the synthesis of high entropy metal sulfide ($(CrMnFeCoNi)S_x$) solid solution NPs through a pulse thermal decomposition method to overcome the immiscibility of multiple metallic constituents in 2021. The obtained $(CrMnFeCoNi)S_x$ NPs were used as electrocatalysts for OER in 1 M KOH solution, and showed a very low overpotential of 295 mV and a good operating stability for 10 hours at 100 mA cm^{-2} current density.

Compared with HEAs, the shape control of HEMs is more difficult to achieve, mainly because the compound phase of different metals is more complex, and it is difficult to achieve consistent kinetic diffusion among each element in the preparation process. Han *et al.*[92] introduced the concept of high entropy to the self-supporting HEO catalyst, which was prepared using a simple and scalable electrodeposition method. In this work, binary NiFe was selected as the initial component of the highly active OER catalyst, and the effect of the composition cutting on the performance of OER was studied by doping Co, Mn and Al. All elements are evenly distributed in the amorphous structure. It was found that the doping of Co and high Mn could improve the conductivity of the catalyst. Doped Al as a sacrificial template is dealloyed in alkaline solution to form nanopore structure, resulting in an increase in electrochemical active surface area. This work is more in line with the previous review article: amorphous materials have unique short-range atomic ordered and long-range disordered structures, which have attracted more and more attention in electrocatalysis,[69] especially in water splitting catalysis. This work provides a compelling demonstration of HEMs as effective OER catalysts, a comprehensive understanding of multi-element synergies, and potential guidance for self-supporting HEMs electrocatalyst design (Fig. 4d). Obviously, structural adjustment is an effective strategy to improve the electrochemical performances of HEMs. However, none of the reported non-precious metal HEMs has achieved the morphology control of nanomaterials, which further indicates that the morphology control of HEMs is a very important scientific direction. Lai *et al.*[36] achieved the controllable preparation of HEOs with different structures by controlling ionic diffusion and oxidation rate. The work was carried out with a simple hydrothermal technique through which five kinds of metal species are uniformly integrated into amorphous carbon spheres that are converted to HEOs by calcination. As shown in Fig. 4e, this work successfully achieved structural regulation from a solid sphere to a core–shell sphere to a hollow sphere. Importantly, the obtained HEOs have a single-crystalline structure, all the elements of HEOs with different structures are evenly distributed and the five metal components can be exchanged at will. Core–shell CrMnFeCoNiO shows the best performance due to its component and structural advantages. This work expands the synthesis of HEMs and provides a rational approach for structural regulation, which makes it have great potential as a high-performance energy storage and conversion material.

4.3 Hydrogen evolution reaction

The abbreviation for electrocatalytic hydrogen evolution reaction is HER. It is the use of a catalyst to produce hydrogen by electrochemical means. Energy and environment are the most important issues related to the sustainable development of human society. 80% of the world's energy demand comes from fossil fuels, which will eventually lead to the exhaustion of fossil fuels, and also lead to serious environmental pollution. It is an inevitable trend to gradually shift from fossil fuels to sustainable non-fossil energy without pollution. Hydrogen is

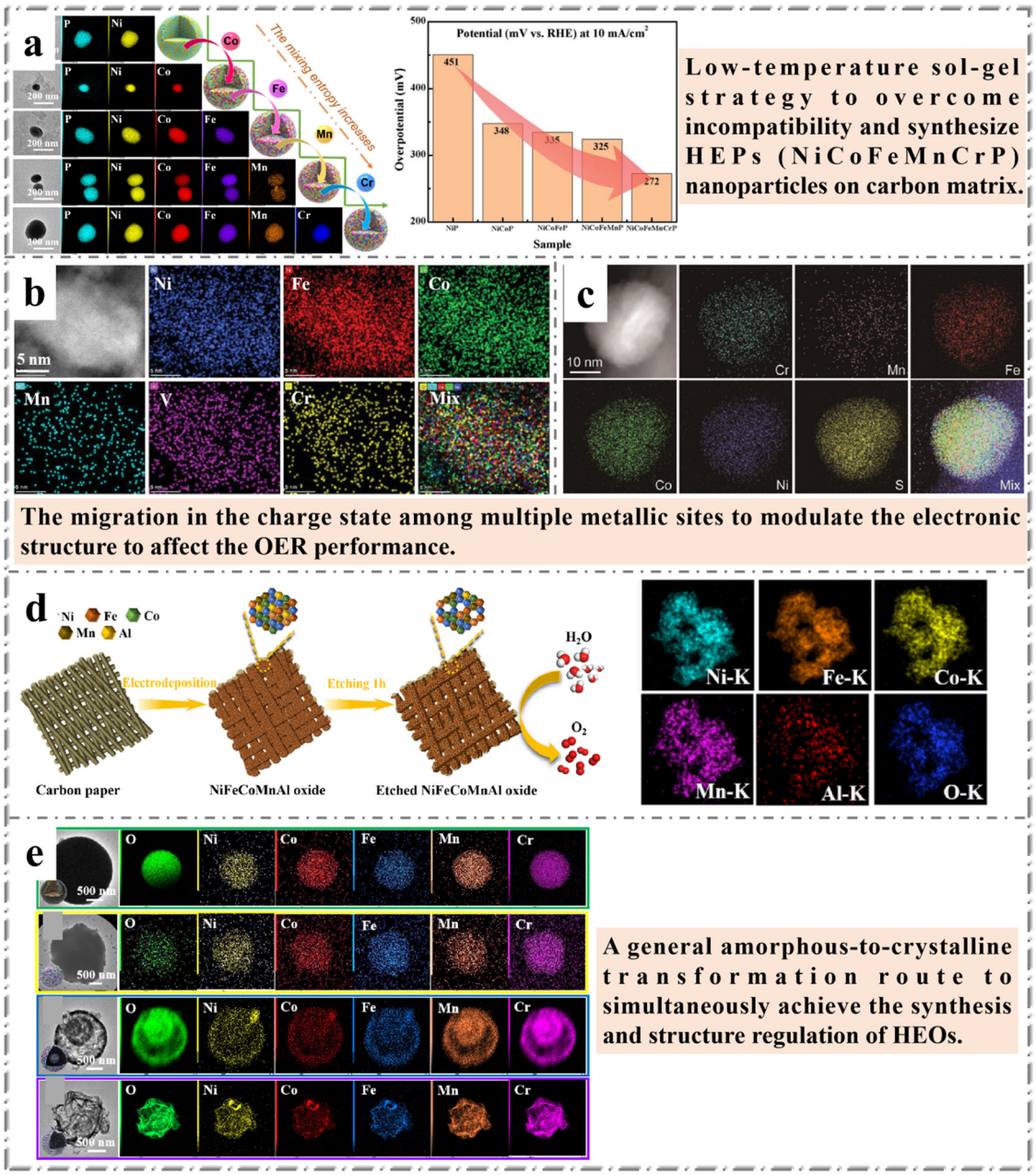

Fig. 4 Examples of HEMs in OER: (a) HEP NiCoFeMnCrP NPs: TEM images, corresponding element mappings and overpotentials for OER of the samples. Reprinted with permission.[31] Copyright 2021, The Royal Society of Chemistry. (b) STEM-HAADF image with corresponding EDX mappings for Fe (red), Ni (blue), Co (green), Cr (yellow), Mn (cyan), and V (magenta) of FeNiCoCrMnV HEO catalysts. Reprinted with permission.[90] Copyright 2022, Wiley-VCH. (c) HAADF-STEM image of a $(CrMnFeCoNi)S_x$ nanoparticle and the corresponding EDS elemental mappings. Reprinted with permission.[91] Copyright 2021, Wiley-VCH. (d) Schematic illustration of the synthetic procedures for nanoporous NiFeCoMnAl oxide grown on carbon paper and corresponding EDS elemental mapping of Ni, Fe, Co, Mn, Al, O for etched NiFeCoMnAl. Reprinted with permission.[92] Copyright 2022, Elsevier Ltd. (e) TEM images and the corresponding element EDS mappings of the CrMnFeCoNiO. Reprinted with permission.[36] Copyright 2023, The Royal Society of Chemistry.

one of the ideal clean energy and an important chemical raw material.[93] Producing hydrogen by electrolytic water splitting is an important means to achieve industrialization and cheap hydrogen production. HER is a semi-reaction of electrocatalytic water splitting, involving the transfer of two proton-coupled electrons ($2H^+ + 2e^- \rightarrow H_2$ in acidic media and $2H_2O + 2e^- \rightarrow H_2 + 2OH^-$ in alkaline solutions), with only one intermediate species (H*) in the rate-determining step. From the Gibbs free energy of hydrogen adsorption on the metal surface, the HER catalysts exhibit good activity when have appropriate combination with reaction intermediates, neither too strong nor too weak.[94] Therefore, HER is mainly used as a model reaction to develop feasible synthesis techniques and probe the structure–function relationship of nanostructured HEMs. Cai *et al.*[95] reported an easy synthesis of nano-porous ultra-high entropy alloys (np-UHEAs) with layered porosity by dealloying.

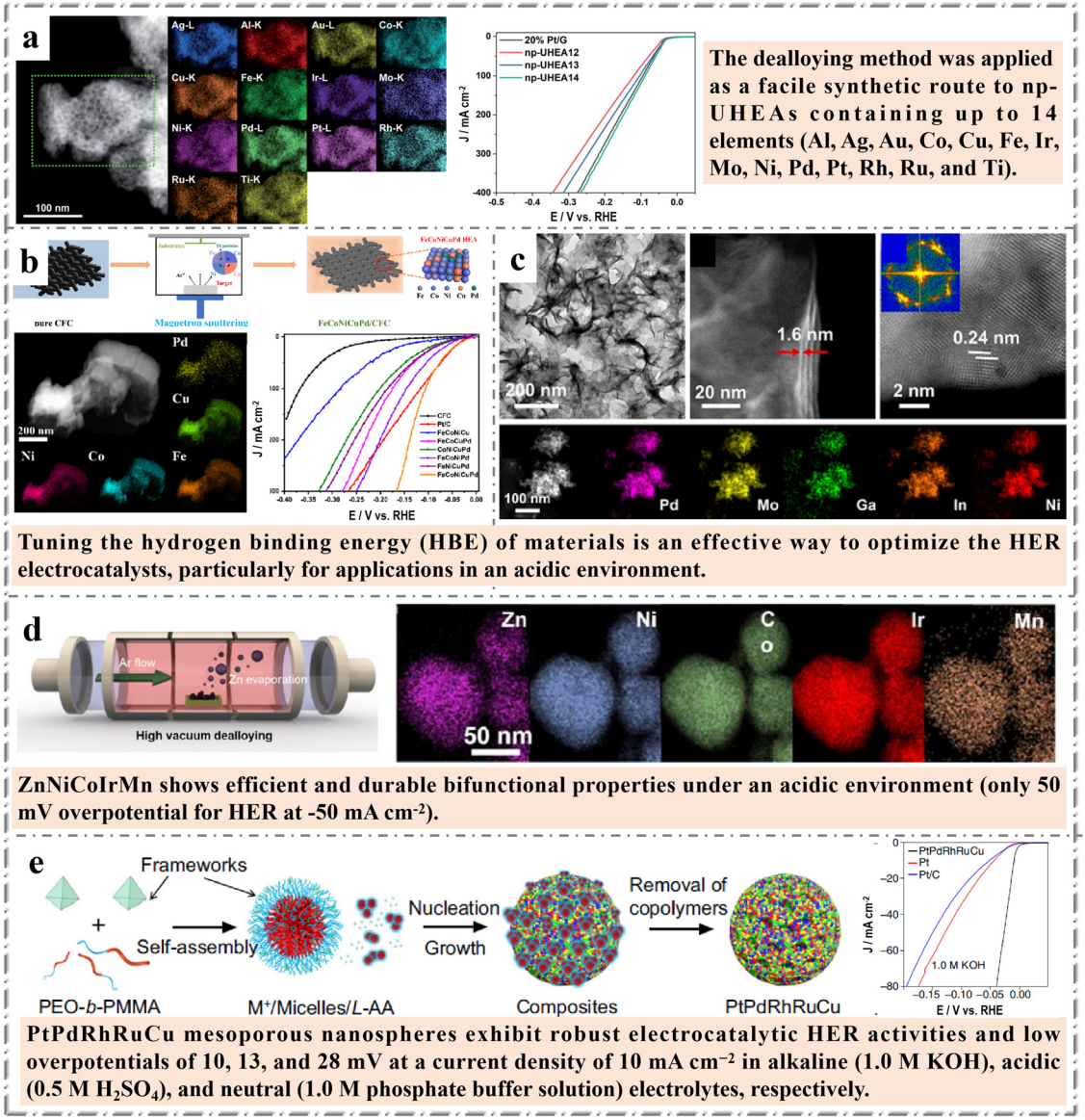

Fig. 5 Examples of HEMs in HER: (a) TEM image, EDX mappings and electrocatalytic performance of np-UHEAs ($Al_{87}Ag_1Au_1Co_1Cu_1Fe_1Ir_1Mo_1Ni_1Pd_1Pt_1Rh_1Ru1Ti_1$). Reprinted with permission.[95] Copyright 2021, The Royal Society of Chemistry. (b) Fabrication schematic illustration, TEM image and corresponding EDX mappings and electrocatalytic performance of the FeCoNiCuPd film. Reprinted with permission.[96] Copyright 2022, Elsevier Ltd. (c) Electron microscopic characterization of high-entropy alloy PdMoGaInNi nanosheets. Reprinted with permission.[97] Copyright 2022, American Chemical Society. (d) Schematic illustration of selective Zn dealloying through vapor dealloying process and EDX mappings of ZnNiCoIrMn). Reprinted with permission.[98] Copyright 2023, Wiley-VCH; (e) Schematic illustration of PtPdRhRuCu mesoporous nanospheres and electrocatalytic performance of samples (polarization curves). Reprinted with permission.[99] Copyright 2023, Springer Nature.

These np-UHEAs contain up to 14 elements, namely Al, Ag, Au, Co, Cu, Fe, Ir, Mo, Ni, Pd, Pt, Rh, Ru, and Ti. This simple dealloying method can directly modify the composition and structure of np-HEAs for a variety of complex reactions. In addition, they show high catalytic activity and electrochemical stability in HER reactions in acidic media, which is superior to existing Pt/graphene (Fig. 5a). This research not only provides the basis for the development and design of HEMs with different compositions and structures, but also provides unprecedented opportunity for the manufacture of omnipotent catalysts for a variety of applications.

On the other hand, HER applications always require some supporting substrate, and the traditional adhesive fixing method will greatly reduce the performance of the catalyst. Therefore, it is very necessary to fix HEMs on the supporting substrate efficiently and easily. Wang *et al.*[96] deposited FeCoNiCuPd with single face-centered cubic structure on carbon fiber cloth (CFC) by magnetron sputtering technology. The FeCoNiCuPd/CFC module exhibits a remarkable electrocatalytic performance with a low overpotential of 29 mV for HER at 10 mA cm^{-2}, superior to commercially available Pt/C. In addition, the novel electrocatalyst also shows impressive HER stability

under high current density conditions. This work provides a feasible method for producing high performance HEMs catalysts for water decomposition (Fig. 5b).

Similarly, the morphology regulation of HEMs is also very challenging in HER catalysts, because the catalysts need to have certain acid and alkaline resistance, and their working environment may be more harsh, which may lead to the adverse effect of structural regulation on the catalytic performance. As shown in Fig. 5c, Fu *et al.*[97] reported the discovery of PdMoGaInNi, a Pt-free group with optimal hydrogen binding energy values, by computer aided screening. As an exploratory example of a two-dimensional HEA for HER, PdMoGaInNi HEA nanosheets have been synthesized to achieve a predicted Pt-free combination with an optimal hydrogen binding energy. The HEA nanosheets were prepared by a traditional oil bath reduction process. PdMoGaInNi HEA nanosheets show high HER activity, with a low overpotential of 13 mV at 10 mA cm^{-2}, superior to commercial Pd/C and Pt/C catalysts. Given the high entropy, lattice distortion and slow diffusion effects of HEA, PdMoGaInNi shows good long-term durability of at least 200 hours in proton exchange membrane water electrolytic cells.

In addition, how to tailor the electronic structure in HEA is also a big challenge. Kwon *et al.*[98] designed Ir-based electrocatalysts using a ZnNiCoIrX HEA platform with two elements (X: Fe and Mn). They achieved easy dealloying through a vacuum system in which Zn was used as a sacrificial element to construct a nanoporous HEA structure with high crystallinity. This work found that the incorporation of Mn into HEA would adjust the electronic structure of Ir site, causing the d-band center to move away from the Fermi level. The downward movement of the d-band center weakens the adsorption energy with the reaction intermediates, which is conducive to catalyzing the reaction. When in the case of low Ir content of the catalyst, HER overpotential is only 50 mV at −50 mA cm^{-2}. ZnNiCoIrMn shows almost constant voltage for HER for 100 h and high stability number of 3.4×10^5 $n_{hydrogen}$ $n_{Ir}{}^{-1}$, demonstrating exceptional durability of HEA platform. The results provide one of the means for the practical preparation of low-cost and efficient nanoporous HEMs electrocatalysts.

At present, more and more researchers believe that it is necessary to design HEMs with specific morphology and composition of nanostructures in order to increase the richness of nanostructures and explore the structure-performance relationship. Recently, Kang *et al.* designed a one-pot wet-chemical reduction approach to synthesize core–shell motif PtPdRhRuCu mesoporous nanospheres (PtPdRhRuCu MMNs) using a diblock copolymer as the soft template (Fig. 5e).[99] Due to the unique morphology and structure, the material with adjustable composition has exposed porous structure and is rich in high entropy alloy potential, and thus exhibits robust electrocatalytic hydrogen evolution reaction (HER) activities and low overpotentials of 10, 13, and 28 mV at a current density of 10 mA cm^{-2} in alkaline (1.0 M KOH), acidic (0.5 M H_2SO_4), and neutral (1.0 M phosphate buffer solution) electrolytes, respectively. This work closely links the concept of HEMs and mesoporous, and further expands the application range of HEMs.

4.4 Carbon dioxide reduction reaction

The energy crisis caused by the depletion of fossil fuels and global warming are two serious challenges.[100] In today's society, the excessive using of energy resources is derived from nonrenewable fossil fuels, and the generated carbon dioxide is one of the main greenhouse gases. In the past decades, great efforts have been made to control carbon dioxide emissions and reduce their impact on the ecological environment. However, the earth's carbon cycle is facing a great challenge due to human's overusing of fossil fuels for their comfortable life. At present, about 40 billion tons of carbon dioxide is generated every year, of which 14% comes from land use and 86% from fossil fuels. About 46 percent of carbon dioxide emitted remains in the atmosphere, while 54 percent is absorbed by ocean and terrestrial carbon sinks.[101,102] Therefore, we need a very large scale of CO_2 capture and conversion in order to protect our living environment. In addition to reduce carbon dioxide production rate, the conversion of carbon dioxide into other carbon-based compounds or fuels can be another complementary and important means for the sustainability and development of human society. The conversion of carbon dioxide into useful chemicals by electrolysis has long been the focus of researchers. In particular, electrochemical conversion of carbon dioxide (ECR) at temperatures below 100 °C is now approaching industrial scale.[103] CO_2 electrochemical reduction also involves multi-electron transfer similar to ORR, but produces a wider range of products, including C_1 products (CO, $HCOO^-$, HCHO, CH_4, CH_3OH, *etc.*), C_{2+} hydrocarbons and oxides, and chemicals containing heteroatoms. In the reaction, water is used as the most common and green electrolyte. The major side reaction from aqueous electrolytes is the water reduction, also known as HER, which can prevail over ECR. Thus, the catalysts need not only accelerate ECR with enhanced efficiency and selectivity toward specific products, but also suppress the competing HER.[100] Therefore, the manufacture of efficient and selective high value-added CO_2 reduction catalysts is very desirable and actively pursued.

Compared to the above electrocatalytic studies (*e.g.* HER, OER and ORR), the design of high entropy ECR catalysts is more difficult, the challenge is that more metal elements may cause the product selectivity disorder. Therefore, the design of a suitable HEMs catalyst requires extremely precise coordination between the components, which is difficult to achieve at the current atomic level of chemical control. Pedersen *et al.*[104] predicted CO and hydrogen (H) adsorption energies at all surface sites on disordered CoCuGaNiZn and AgAuCuPdPt HEAs (111) surfaces by combining DFT with supervised machine learning (Fig. 6a). Through their simulation and calculation, they found that necessary (but by no means sufficient) criteria were used for weak H adsorption and strong CO adsorption. This work presented a framework for unbiased discovery of new catalyst candidates for CO_2RR and CORR, using two disordered HEAs CoCuGaNiZn and AgAuCuPdPt as starting points. Knowing only the catalytic properties of Cu, the model can suggest, for example, that GaNi as a locally optimal catalyst candidate for CO_2RR/CORR is known experimentally to

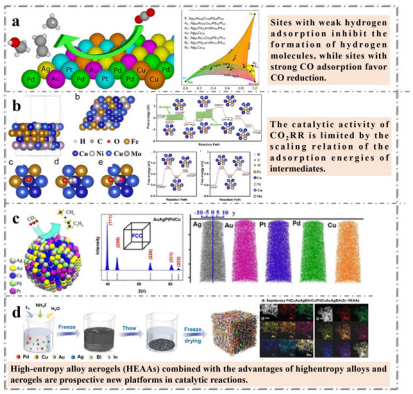

Fig. 6 Examples of HEMs in CO_2RR: (a) schematic diagram of catalytic reaction of HEA (AgAuCuPdPt) and selectivity–activity plots (plot of the CO_2RR/CORR selectivity and CORR activity space achievable of HEA (AgAuCuPdPt). Reprinted with permission.[104] Copyright 2020, American Chemical Society. (b) The active surface of HEAs ($Fe_{0.2}Co_{0.2}Ni_{0.2}$-$Cu_{0.2}Mo_{0.2}$ (111)), structures of the designed three active sites and adsorption configuration of CHO* on Ni–Mo and Ni–Cu sites of HEAs with the charge density difference and simulated reaction of CO_2RR on HEAs. Reprinted with permission.[105] Copyright 2022, American Chemical Society. (c) Schematic of the catalysis reaction, XRD pattern of HEA alloy NPs (AuAgPtPdCu) and mapping of an atom probe microscope. Reprinted with permission.[106] Copyright 2022, American Chemical Society. (d) Schematic illustration of the preparation and STEM-EDS elemental mappings of PdCuAuAgBiIn HEAAs. Reprinted with permission.[107] Copyright 2022, Wiley-VCH.

exhibit a degree of selectivity for highly reduced carbon products. This demonstrates the model's ability to predict effective catalyst candidates without prior knowledge of catalyst performance, and provides a method for probabilistically optimizing disordered alloy composition for optimal catalytic performance.

In order to further improve the ECR catalytic performance of HEMs, Chen *et al.*[105] proposed that circumventing the scale relationship is a breakthrough in catalytic activity. They designed FeCoNiCuMo HEA system with high catalytic activity based on DFT calculations. The Vienna *ab initio* simulation package (VASP) was applied to perform spin-polarized DFT calculations. The core electrons were described by the projectoraugmented wave pseudopotential and the generalized gradient approximation (GGA) with the Perdew–Burke–Ernzerhof functional (PBE) was considered for all DFT calculations. The high entropy alloy structures were built by a neural evolution structure (NES) generation methodology. Based on 1280 adsorption sites, a machine learning model was established to predict the adsorption energies of COOH*, CO* and CHO*. The rotation of COOH*, CO* and CHO* on the surface of the designed HEA avoids the scaling relationship of the adsorption energies of COOH*, CO* and CHO*, and CO_2RR has excellent catalytic activity with a limit potential of 0.29–0.51 V (Fig. 6b). This work not only accelerates the development of HEA catalyst, but also provides an effective strategy to avoid scaling relationship.

With a theoretical basis, Nellaiappan *et al.*[106] used a nanocrystalline HEA (AuAgPtPdCu) to convert CO_2 into gaseous hydrocarbons. They prepared HEAs by forming a solid solution at high temperature. At low application potential (−0.3 V *vs.* reversible hydrogen electrode), the faradaic efficiency for gaseous products is about 100% (Fig. 6c). Li *et al.*[107] reported the preparation of a series of high-entropy alloy aerogels (HEAAs) by freeze–thaw method as highly active and durable electrocatalysts for CO_2RR (Fig. 6d). PdCuAuAgBiIn HEAAs can achieve almost 100% faradaic efficiency (FE) for C_1 products between −0.7 and −1.1 V, and 98.1% FE for formic acid at −1.1 V. It is better than PdCuAuAgBiIn HEAs and Pd metallic aerogel (MAs) reported. As shown in Fig. 6d, compared with the reported HEA, HEAAs have more pore structure, which means it has more effective active sites, adsorption capacity of reactants and desorption capacity of products. This work not only provides a simple synthesis strategy for the preparation of HEAAs, but also opens the way for the development of efficient catalysts.

4.5 Alcohol oxidation reaction

Fuel cell is a kind of chemical device which converts the chemical energy of fuel directly into electric energy, also known as electrochemical generator. It is the fourth generation technology after hydropower, thermal power and atomic power. Because the Gibbs free energy in the chemical energy of fuel is converted into electric energy by electrochemical reaction, the fuel cell is not restricted by Carnot cycle effect, so the efficiency is high. In addition, fuel cells have a long service life because they use fuel and oxygen as raw materials and have no mechanical transmission parts. Thus, from the perspective of saving energy and protecting the ecological environment, fuel cell is the most promising power generation technology. Methanol and ethanol are two common direct alcohol fuel cells (DAFCs).[108] Many previous studies have reported that platinum group metals, including Ru, Rh, Pd, Os, Ir, and Pt, have been widely used as electrocatalysts for alcohol oxidation. While mono-metal and bimetallic platinum group metals can trigger simple reactions, it is difficult to drive complex reactions involving multiple proton-electron transfers and intermediate species.[109] The excellent corrosion resistance and strong polymetallic synergism make HEMs as an ideal catalyst for the efficient complete oxidation of alcohol fuel.

Li *et al.*[110] reported a dealloying process for a nanoporous multi-component anode and cathode catalyst for high performance ethanol fuel cells. As shown in Fig. 7a, on the anode side, the porous AlPdNiCuMo alloy showed electrochemical activity of 88.53 $m^2\ g_{Pd}^{-1}$ and mass activity of 2.67 A mg_{Pd}^{-1} during the ethanol oxidation reaction. At the cathode side, dealloying spinel $(AlMnCo)_3O_4$ nanocrystalline sheets without noble metals showed comparable catalytic performance to standard Pt/C in oxygen reduction reaction, and showed tolerance to high concentration of ethanol. Flexible solid ethanol fuel cells, equipped with such anode and cathode catalysts, provide an ultra-high energy density of 13.63 mW h cm^{-2} with just 3 mL ethanol, which is outstanding compared to other similar solid energy devices.

Similarly, this catalytic reaction is focused on practical applications, so HEMs catalysts need to be supported on certain substrates or self-supported. Fan *et al.*[111] reported a simple method to prepare high entropy PdPtCuAgAu nanowire

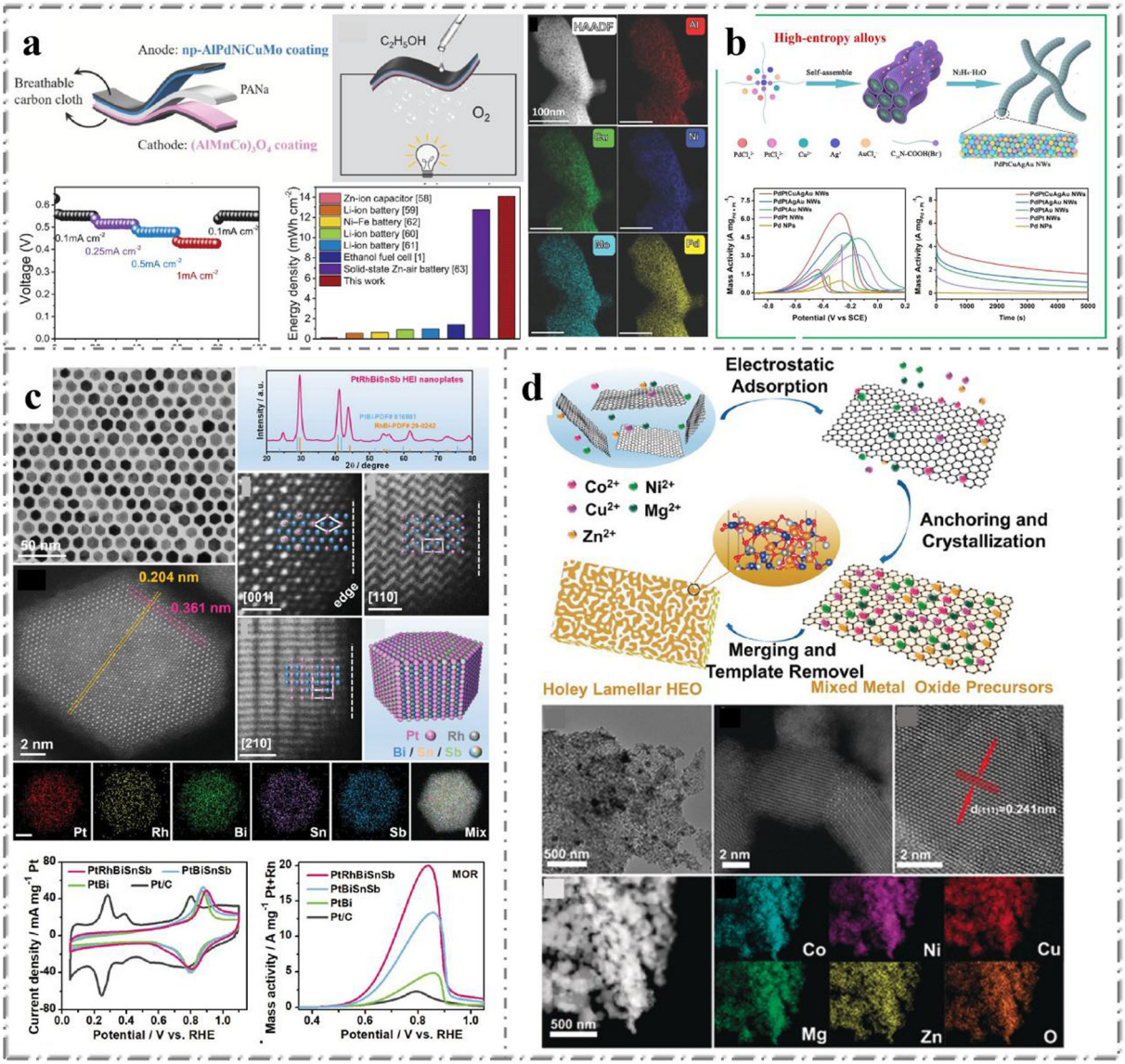

Fig. 7 Examples of HEMs in alcohol oxidation: (a) schematic and catalytic performance characterization of flexible solid-state AlPdNiCuMo. Reprinted with permission.[110] Copyright 2020, Wiley-VCH. (b) Schematic illustration and catalytic performance characterization of PdPtCuAgAu HEA NWs. Reprinted with permission.[111] Copyright 2022, Elsevier Ltd. (c) TEM image, XRD pattern and catalytic performance of the PtRhBiSnSb HEI nanoplates. Reprinted with permission.[112] Copyright 2022, Wiley-VCH. (d) TEM, HRTEM images and elemental mappings of $Co_{0.2}Ni_{0.2}Cu_{0.2}Mg_{0.2}Zn_{0.2}O$. Reprinted with permission.[113] Copyright 2020, Wiley-VCH.

networks using carboxyl functionalized surfactants as soft templates (Fig. 7b). The PdPtCuAgAu alloy electrocatalyst has high mass activity (7.7 A mg_{Pd+Pt}^{-1}), good stability/durability, anti-poisoning ability and good electrocatalytic kinetics, which significantly improves the electrocatalytic performance of ethanol oxidation reaction. This method for the synthesis of HEAs will provide a new approach for the rational design of other high entropy nanocatalysts with ideal morphology/structure and function for a wide range of catalytic applications.

On the other hand, the control of catalyst composition needs to be more precise and variable in practical application. The elements in most reported HEMs are basically located in the same group or have similar atomic radius, so it is relatively easy to achieve synthesis. However, it is difficult to synthesize and regulate HEMs with large differences in atomic radius. Chen *et al.*[112] recently reported a one-pot synthesis of hexagonal tightly packed (hcp) PtRhBiSnSb high entropy intermetallic compound (HEI) nanoplates with intrinsically isolated Pt, Rh, Bi, Sn, and Sb atoms to facilitate the electrochemical oxidation of liquid fuels (Fig. 7c). Using the combination of these five metals, the PtRhBiSnSb HEI nanoplates show significant mass activity of 19.529, 15.558 and 7.535 A mg_{Pt+Rh}^{-1} for the electrooxidation of methanol, ethanol and glycerol in alkaline electrolyte, respectively. They found that PtRhBiSnSb HEI achieves record methanol oxidation reaction (MOR) activity in an alkaline environment. This work provides an important research

Table 1 Summary of HEMs for electrocatalysis including ORR, OER, HER, ECR and EOR

Material	Synthesis method	Catalytic reaction	Catalytic performance	Ref.
$Pt_{34}Fe_5Ni_{20}Cu_{31}Mo_9Ru$	One-pot of oil bath	ORR	$E_{1/2}$ (*V vs.* RHE) 0.87 V	80
PdCuPtNiCo	Ion exchange	ORR	$E_{1/2}$ (*V vs.* RHE) 0.86 V	81
$PtPdAuAgCuIrRu@(AlNiCoFeCrMoTi)_3O_4$	Alloying–dealloying	ORR	$E_{1/2}$ (*V vs.* RHE) 0.61 V	25
PtRuFeCoNi@Pt	*In situ* growth	ORR	$E_{1/2}$ (*V vs.* RHE) 0.85 V	82
NiCoFeMnCrP	Sol–gel	OER	Overpotential 270 mV (10 mA cm^{-2})	31
(FeNiCoCrMnV) HEO	Rapid Joule heating and quenching	OER	Overpotential 247 mV (10 mA cm^{-2})	90
$(CrMnFeCoNi)S_x$	Pulse thermal decomposition	OER	Overpotential 247 mV (10 mA cm^{-2})	91
NiFeCoMnAl oxide	Electrodeposition	OER	Overpotential 190 mV (10 mA cm^{-2})	92
np-UHEAs (14 elements)	One-step dealloying	HER	Overpotential 32 mV (10 mA cm^{-2})	95
FeCoNiCuPd	Magnetron sputtering	HER	Overpotential 29 mV (10 mA cm^{-2})	96
PdMoGaInNi	Oil bath	HER	Overpotential 13 mV (10 mA cm^{-2})	97
ZnNiCoIrMn	Calcining method	HER	Overpotential 50 mV (50 mA cm^{-2})	98
AuAgPtPdCu	Melting method	ECR	*E* (*V vs.* RHE) −0.3 V $FE_{(CH_4)}$ 49.4%	106
PdCuAuAgBiIn	Freeze–thaw method	ECR	*E* (*V vs.* RHE) −1.1 V $FE_{(HCOOH)}$ 98.1%	107
RuRhPdOsIrPt	Wet chemical synthesis	EOR	E_{onset} (*V vs.* RHE) 0.28 V (50 mV s^{-1})	109

advance for the development of HEMs with fine control of composition and properties, further expanding the membership of the HEMs family. In addition, HEMs also play an important role in catalytic oxidation of organic alcohols. Feng *et al.*[113] prepared a porous layered HEO ($Co_{0.2}Ni_{0.2}Cu_{0.2}Mg_{0.2}Zn_{0.2}O$) material with a mesoporous structure using an anchoring consolidation process (Fig. 7d). The HEO catalyst has high catalytic activity for solvent-free aerobic oxidation of benzyl alcohol and can achieve 98% conversion within 2 hours, which is the highest conversion rate of benzyl alcohol oxidation to date. By adjusting the catalytic reaction parameters, benzoic acid or benzaldehyde can be selectively optimized as the main products. This study is of great significance for the utilization of HEO materials with unique structure and provides a prospect for the development of multiphase catalysts in industrial catalysis field.

5 Conclusion and outlook

HEMs have been developed rapidly in synthesis, composition/morphology control and electrochemical reaction applications as summarized in Table 1. The superior catalytic performance of HEMs can be attributed to the four effects mentioned above. The underlying reason is that the restriction of five or more metal species on the atomic scale collaboratively changes the electronic and geometric characteristics of the HEMs surface and the immeasurable cocktail effect of multiple element combinations. On the other hand, the diversity of structures also greatly improves the catalytic performance of HEMs. Thus, different surface sites and shape features introduce a wide range of adsorption energy into intermediates, providing more opportunities for regulating activity and selectivity. This is particularly useful for optimizing reactions involving multiple charge transfers, such as electrochemical reactions for carbon dioxide reduction and alcohol oxidation. In addition, the generally excellent catalytic stability of HEMs has been considered to be the result of entropy-induced stability, which may be a complex subject requiring more research. In conclusion, much progress has been made in the study of HEMs, but to advance further, as described below, continued efforts are needed in many areas, such as synthesis methodology, advanced characterization, basic understanding, and applications.

Precisely controlled synthesis is currently the most explored aspect of HEMs, and more precise and purposeful design is now required. Considering the immiscibility in HEMs due to element differences and composition complexity, synthesis must continue to rely on temperature, force, pressure, energy field and other non-equilibrium methods to achieve uniform mixing and small particle size. But we do not believe that these conditions are necessarily sufficient and necessary. The successful preparation of HEAs single crystal nanosheets by controlled synthesis at room temperature has been reported.[34] This breakthrough also means that the synthesis method of HEMs is not limited to extreme environments. We still need to explore how to balance non-equilibrium synthesis with subtle structural or morphological controls in terms of size, phase, shape and surface decoration, which will require considerable effort and knowledge gained from existing chemical synthesis in various fields.

What is lacking in HEMs research at present is a basic understanding of the controllability of surface, intrinsic defects and element distribution in high entropy NPs, which will have great guiding significance for catalytic performance. Most studies do not involve the separation of surface or interfacial elements, the reconstruction of crystal phase, and the reconstruction of electronic structures, especially the dynamic evolution of their components under catalytic conditions, which is particularly important. To overcome these difficulties, it is necessary to introduce more advanced characterization techniques, such as a new transscale imaging method for AFM and scanning microlens associated microscopy,[114] Terahertz scanning tunneling microscope system,[115] small-molecule serial femtosecond X-ray crystallography,[116] *in situ* liquid transmission electron microscopy[117] and so on. More information, such as surface atomic structure evolution, lattice strain, atomic diffusion behavior and electronic structure of each atom, can

be obtained through more advanced techniques to provide reliable basis for theoretical simulation/theoretical calculation and understanding of the formation mechanism.

HEMs show great promises for high performance catalysis, especially for complex reactions that require different combinations of active sites. However, how to properly design HEMs to best suit these response schemes remains a challenging scientific issue. In addition, it is not clear how to identify the active site and understand the source of performance. Most of the current research on HEMs is based on traditional catalysts, but the active sites of HEMs do not match them, and its four effects may lead to unimaginable new active sites. Among them, high entropy effect and cocktail effect bring the most obvious unpredictability. This is mainly related to the severe lattice distortion of the crystal structure of HEMs and the unpredictable cocktail effect, the existence of which may lead to the creation of unpredictable new active sites in HEMs. At this point, there is no theoretical research to achieve accurate performance prediction of each element combination of HEMs. We believe that a more cohesive effort is needed to link the chemistry, physics, and materials communities to introduce a new frontier in the discovery and design of highly efficient catalytic materials.

Conflicts of interest

The authors declare no competing interests.

Acknowledgements

This work is supported by the National Natural Science Foundation of China (Grant No. 22175084, 22275082 and 21871130), Scientific and Technological Innovation Project of Carbon Emission Peak and Carbon Neatrality of Jiangsu Province (Grant No. BE2022024) and the Postgraduate Research & Practice Innovation Program of Jiangsu Province (SJCX22_0024).

References

1 S. S. Aamlid, M. Oudah, J. Rottler and A. M. Hallas, *J. Am. Chem. Soc.*, 2023, **145**, 5991–6006.
2 E. P. George, D. Raabe and R. O. Ritchie, *Nat. Rev. Mater.*, 2019, **4**, 515–534.
3 J. W. Yeh, S. K. Chen, S. J. Lin, J. Y. Gan, T. S. Chin, T. T. Shun, C. H. Tsau and S. Y. Chang, *Adv. Eng. Mater.*, 2004, **6**, 299–303.
4 B. Cantor, I. T. H. Chang, P. Knight and A. J. B. Vincent, *Mater. Sci. Eng., A*, 2004, **375–377**, 213–218.
5 M. I. Page, *Angew. Chem., Int. Ed. Engl.*, 1977, **16**, 449–459.
6 Z. T. Mao and C. T. Campbell, *ACS Catal.*, 2019, **9**, 9465–9473.
7 J. Leduc, M. Frank, L. Jürgensen, D. Graf, A. Raauf and S. Mathur, *ACS Catal.*, 2019, **9**, 4719–4741.
8 Y. F. Sun and S. Dai, *Sci. Adv.*, 2021, **7**, eabg1600.
9 G. L. Zhu, Z. H. Huang, Z. Y. Xu and L. T. Yan, *Acc. Chem. Res.*, 2018, **51**, 900–909.
10 J. F. M. Denayer, R. A. Ocakoglu, I. C. Arik, C. E. A. Kirschhock, J. A. Martens and G. V. Baron, *Angew. Chem., Int. Ed.*, 2005, **44**, 400–403.
11 O. E. Atwani, H. T. Vo, M. A. Tunes, C. Lee, A. Alvarado, N. Krienke, J. D. Poplawsky, A. A. Kohnert, J. Gigax, W. Y. Chen, M. Li, Y. Q. Wang, J. S. Wrobel, D. Nguyen-Manh, J. K. S. Baldwin, O. U. Tukac, E. Aydogan, S. Fensin and E. Martinez, *Nat. Commun.*, 2023, **14**, 2516.
12 T. Jin, X. H. Sang, R. R. Unocic, R. T. Kinch, X. F. Liu, J. Hu, H. L. Liu and S. Dai, *Adv. Mater.*, 2018, **30**, 1707512.
13 K. Mori, N. Hashimoto, N. Kamiuchi, H. Yoshida, H. Kobayashi and H. Yamashita, *Nat. Commun.*, 2021, **12**, 3884.
14 S. S. Sohn, A. K. da Silva, Y. Ikeda, F. Kormann, W. J. Lu, W. S. Choi, B. Gault, D. Ponge, J. Neugebauer and D. Raabe, *Adv. Mater.*, 2019, **31**, 1807142.
15 K. Wang, W. B. Hua, X. H. Huang, D. Stenzel, J. B. Wang, Z. M. Ding, Y. Y. Cui, Q. S. Wang, H. Ehrenberg, B. Breitung, C. Kubel and X. K. Mu, *Nat. Commun.*, 2023, **14**, 1487.
16 Y. Yu, W. J. Cui, Z. Q. Xu, S. Wang, W. S. Jiang, R. J. Sun, L. H. Qi and K. Pan, *J. Colloid Interface Sci.*, 2023, **639**, 193–202.
17 X. X. Wei, B. Zhang, B. Wu, Y. J. Wang, X. H. Tian, L. X. Yang, E. E. Oguzie and X. L. Ma, *Nat. Commun.*, 2022, **13**, 726.
18 M. A. Buckingham, B. Ward-O'Brien, W. C. Xiao, Y. Li, J. Qu and D. J. Lewis, *Chem. Commun.*, 2022, **58**, 8025–8037.
19 L. J. Zhang, W. W. Cai, N. Z. Bao and H. Yang, *Adv. Mater.*, 2022, **34**, 2110511.
20 F. Marques, M. Balcerzak, F. Winkelmann, G. Zepon and M. Felderhoff, *Energy Environ. Sci.*, 2021, **14**, 5191–5227.
21 Y. D. Gao, Z. M. Qiu, Y. Lu, H. J. Zhou, R. M. Zhu, Z. Liu and H. Pang, *Inorg. Chem.*, 2023, **62**, 3669–3678.
22 N. K. Katiyar, K. Biswas, J. W. Yeh, S. Sharma and C. S. Tiwary, *Nano Energy*, 2021, **88**, 106261.
23 D. S. Wu, K. Kusada, T. Yamamoto, T. Toriyama, S. Matsumura, I. Gueye, O. Seo, J. Kim, S. Hiroi, O. Sakata, S. Kawaguchi, Y. Kubota and H. Kitagawa, *Chem. Sci.*, 2020, **11**, 12731–12736.
24 B. Jiang, H. R. Xue, P. Wang, H. R. Du, Y. Q. Kang, J. J. Zhao, S. Y. Wang, W. Zhou, Z. F. Bian, H. X. Li, J. Henzie and Y. Yamauchi, *J. Am. Chem. Soc.*, 2023, **145**, 6079–6086.
25 Z. Y. Jin, X. Y. Zhou, Y. X. Hu, X. W. Tang, K. L. Hu, K. M. Reddy, X. Lin and H. J. Qiu, *Chem. Sci.*, 2022, **13**, 12056–12064.
26 Z. T. Fang, M. P. Confer, Y. X. Wang, Q. Wang, M. R. Kunz, E. J. Dufek, B. Liaw, T. M. Klein, D. A. Dixon and R. Fushimi, *J. Am. Chem. Soc.*, 2021, **143**, 10261–10274.
27 C. C. Kong, W. J. Lei, B. S. Lei, F. Z. Pu, G. Wang, X. J. Zhang, C. Zhou and Z. M. Yang, *Langmuir*, 2021, **37**, 10987–10993.
28 Z. P. Wang, Z. P. Lin, Y. L. Wang, S. J. Shen, Q. H. Zhang, J. C. Wang and W. W. Zhong, *Adv. Mater.*, 2023, **35**, 2302007.

29 P. C. Chen, X. l Liu, J. L. Hedrick, Z. Xie, S. Z. Wang, Q. Y. Lin, M. C. Hersam, V. P. Dravid and C. A. Mirkin, *Science*, 2016, **352**, 1565–1569.
30 Y. G. Yao, Z. N. Huang, P. F. Xie, S. D. Lacey, R. J. Jacob, H. Xie, F. J. Chen, A. M. Nie, T. C. Pu, M. Rehwoldt, D. W. Yu, M. R. Zachariah, C. Wang, R. Shahbazian-Yassar, J. Li and L. B. Hu, *Science*, 2018, **359**, 1489–1494.
31 D. W. Lai, Q. L. Kang, F. Gao and Q. Y. Lu, *J. Mater. Chem. A*, 2021, **9**, 17913–17922.
32 Y. G. Yao, Z. N. Huang, L. A. Hughes, J. L. Gao, T. Y. Li, D. Morris, S. E. Zeltmann, B. H. Savitzky, C. Ophus, Y. Z. Finfrock, Q. Dong, M. L. Jiao, Y. M. Mao, M. F. Chi, P. Zhang, J. Li, A. M. Minor, R. Shahbazian-Yassar and L. B. Hu, *Matter*, 2021, **4**, 2340–2353.
33 K. Z. Gu, D. P. Wang, C. Xie, T. H. Wang, G. Huang, Y. B. Liu, Y. Q. Zou, L. Tao and S. Y. Wang, *Angew. Chem., Int. Ed.*, 2021, **60**, 20253–20258.
34 L. Tao, M. Z. Sun, Y. Zhou, M. C. Luo, F. Lv, M. G. Li, Q. H. Zhang, L. Gu, B. L. Huang and S. J. Guo, *J. Am. Chem. Soc.*, 2022, **144**, 10582–10590.
35 M. Du, P. B. Geng, C. X. Pei, X. Y. Jiang, Y. Y. Shan, W. H. Hu, L. B. Ni and H. Pang, *Angew. Chem., Int. Ed.*, 2022, **61**, 202209350.
36 D. W. Lai, L. Ling, M. F. Su, Q. Kang, F. Gao and Q. Y. Lu, *Chem. Sci.*, 2023, **14**, 1787–1796.
37 X. Z. Wang, Q. Dong, H. Y. Qiao, Z. N. Huang, M. T. Saray, G. Zhong, Z. W. Lin, M. J. Cui, A. Brozena, M. Hong, Q. Q. Xia, J. L. Gao, G. Chen, R. Shahbazian-Yassar, D. W. Wang and L. B. Hu, *Adv. Mater.*, 2020, **32**, 2002853.
38 J. J. Calvin, T. M. Kaufman, A. B. Sedlak, M. F. Crook and A. P. Alivisatos, *Nat. Commun.*, 2021, **12**, 2663.
39 M. Resano, M. Aramendia, E. Garcia-Ruiz, A. Bazo, E. Bolea-Fernandez and F. Vanhaecke, *Chem. Sci.*, 2022, **13**, 4436–4473.
40 H. Y. Wang, M. Soldemo, D. Degerman, P. Lomker, C. Schlueter, A. Nilsson and P. Amann, *Angew. Chem., Int. Ed.*, 2022, **61**, 202111021.
41 H. Asakura, S. Hosokawa, T. Ina, K. Kato, K. Nitta, K. Uera, T. Uruga, H. Miura, T. Shishido, J. Ohyama, A. Satsuma, K. Sato, A. Yamamoto, S. Hinokuma, H. Yoshida, M. Machida, S. Yamazoe, T. Tsukuda, K. Teramura and T. Tanaka, *J. Am. Chem. Soc.*, 2018, **140**, 176–184.
42 C. L. Hall, J. Potticary, V. Hamilton, S. Gaisford, A. Buanz and S. R. Hall, *Chem. Commun.*, 2020, **56**, 10726–10729.
43 M. N. Banis, H. Yadegari, Q. Sun, T. Regier, T. Boyko, J. G. Zhou, Y. M. Yiu, R. Y. Li, Y. F. Hu, T. K. Sham and X. L. Sun, *Energy Environ. Sci.*, 2018, **11**, 2073–2077.
44 G. Feng, F. H. Ning, J. Song, H. F. Shang, K. Zhang, Z. P. Ding, P. Gao, W. S. Chu and D. G. Xia, *J. Am. Chem. Soc.*, 2021, **143**, 17117–17127.
45 L. Dong, J. B. Zang, W. P. Wang, X. Liu, Y. Zhang, J. Su, Y. H. Wang, X. M. Han and J. S. Li, *J. Colloid Interface Sci.*, 2020, **564**, 134–142.
46 C. Huck-Iriart, L. Soler, A. Casanovas, C. Marini, J. Prat, J. Llorca and C. Escudero, *ACS Catal.*, 2018, **8**, 9625–9636.
47 G. E. Cutsail III, R. Banerjee, A. Zhou, L. Que Jr., J. D. Lipscomb and S. DeBeer, *J. Am. Chem. Soc.*, 2018, **140**, 16807–16820.
48 J. B. Metson, S. J. Hay, H. J. Trodahl, B. Ruck and Y. Hu, *Curr. Appl. Phys.*, 2004, **4**, 233–236.
49 C. W. Andersen, E. Borfecchia, M. Bremholm, M. R. V. Jorgensen, P. N. R. Vennestrom, C. Lamberti, L. F. Lundegaard and B. B. Iversen, *Angew. Chem., Int. Ed.*, 2017, **56**, 10367–10372.
50 A. M. Flank, M. Weininger, L. E. Mortenson and S. P. Cramer, *J. Am. Chem. Soc.*, 1986, **108**, 1049–1055.
51 V. L. Sushkevich, O. V. Safonova, D. Palagin, M. A. Newton and J. A. van Bokhoven, *Chem. Sci.*, 2020, **11**, 5299–5312.
52 P. Eisenberger and B. M. Kincaid, *Science*, 1978, **200**, 1441–1447.
53 J. L. Liu, Y. Q. Li, Z. Chen, N. Liu, L. L. Zheng, W. X. Shi and X. Wang, *J. Am. Chem. Soc.*, 2022, **144**, 23191–23197.
54 L. Su, H. Huyan, A. Sarkar, W. P. Gao, X. X. Yan, C. Addiego, R. Kruk, H. Hahn and X. Q. Pan, *Nat. Commun.*, 2022, **13**, 2358.
55 X. D. Xu, P. Liu, Z. Tang, A. Hirata, S. X. Song, T. G. Nieh, P. K. Liaw, C. T. Liu and M. W. Chen, *Acta Mater.*, 2018, **144**, 107–115.
56 J. H. Zhou, Y. Yang, Y. Yang, D. S. Kim, A. Yuan, X. Z. Tian, C. Ophus, F. Sun, A. K. Schmid, M. Nathanson, H. Heinz, Q. An, H. Zeng, P. Ercius and J. W. Miao, *Nature*, 2019, **570**, 500–503.
57 X. Y. Liu, A. Ronne, L. C. Yu, Y. Liu, M. Y. Ge, C. H. Lin, B. Layne, P. Halstenberg, D. S. Maltsev, A. S. Ivanov, S. Antonelli, S. Dai, W. K. Lee, S. M. Mahurin, A. I. Frenkel, J. F. Wishart, X. H. Xiao and Y. K. Chen-Wiegart, *Nat. Commun.*, 2021, **12**, 3441.
58 K. F. Heinrich, C. Fiori and H. Yakowitz, *Science*, 1970, **167**, 1129–1131.
59 K. H. Downing, *Science*, 1991, **251**, 53–59.
60 A. V. Crewe, *Science*, 1983, **221**, 325–330.
61 C. H. Jin, E. C. Regan, A. M. Yan, M. I. B. Utama, D. Q. Wang, S. H. Zhao, Y. Qin, S. J. Yang, Z. R. Zheng, S. Y. Shi, K. Watanabe, T. Taniguchi, S. Tongay, A. Zettl and F. Wang, *Nature*, 2019, **569**, 76–80.
62 J. Sun, Q. Li, H. Zhu, Z. N. Liu, K. Lin, N. Wang, Q. H. Zhang, L. Gu, J. X. Deng, J. Chen and X. R. Xing, *Adv. Mater.*, 2020, **32**, 2002968.
63 S. C. McGuire, A. M. Ebrahim, N. Hurley, L. Zhang, A. I. Frenkel and S. S. Wong, *Chem. Sci.*, 2021, **12**, 7158–7173.
64 G. Haberfehlner, F. P. Schmidt, G. Schaffernak, A. Horl, A. Trugler, A. Hohenau, F. Hofer, J. R. Krenn, U. Hohenester and G. Kothleitner, *Nano Lett.*, 2017, **17**, 6773–6777.
65 Y. G. Yao, Q. Dong, A. Brozena, J. Luo, J. W. Miao, M. F. Chi, C. Wang, I. G. Kevrekidis, Z. J. Ren, J. Greeley, G. F. Wang, A. Anapolsky and L. B. Hu, *Science*, 2022, **376**, eabn3103.
66 Y. Yang, C. C. Chen, M. C. Scott, C. Ophus, R. Xu, A. Pryor, L. Wu, F. Sun, W. Theis, J. H. Zhou, M. Eisenbach,

P. R. Kent, R. F. Sabirianov, H. Zeng, P. Ercius and J. W. Miao, *Nature*, 2017, **542**, 75–79.
67 Z. W. Chen, L. X. Chen, Z. Wen and Q. Jiang, *Phys. Chem. Chem. Phys.*, 2019, **21**, 23782–23802.
68 L. J. Santodonato, P. K. Liaw, R. R. Unocic, H. Bei and J. R. Morris, *Nat. Commun.*, 2018, **9**, 4520.
69 Q. L. Kang, D. W. Lai, W. Y. Tang, Q. Y. Lu and F. Gao, *Chem. Sci.*, 2021, **12**, 3818–3835.
70 Y. Q. Wang, S. A. Skaanvik, X. Y. Xiong, S. Y. Wang and M. D. Dong, *Matter*, 2021, **4**, 3483–3514.
71 Z. X. Liang, L. Song, S. Q. Deng, Y. M. Zhu, E. Stavitski, R. R. Adzic, J. Y. Chen and J. X. Wang, *J. Am. Chem. Soc.*, 2019, **141**, 9629–9636.
72 N. K. Katiyar, S. Dhakar, A. Parui, P. Gakhad, A. K. Singh, K. Biswas, C. S. Tiwary and S. Sharma, *ACS Catal.*, 2021, **11**, 14000–14007.
73 H. J. Qiu, G. Fang, J. J. Gao, Y. R. Wen, J. Lv, H. L. Li, G. Q. Xie, X. J. Liu and S. H. Sun, *ACS Mater. Lett.*, 2019, **1**, 526–533.
74 D. Roy, S. C. Mandal and B. Pathak, *J. Phys. Chem. Lett.*, 2022, **13**, 5991–6002.
75 A. C. Chen and C. Ostrom, *Chem. Rev.*, 2015, **115**, 11999–12044.
76 Q. Q. Zhang and J. Q. Guan, *Adv. Funct. Mater.*, 2020, **30**, 2000768.
77 K. Zeng, X. J. Zheng, C. Li, J. Yan, J. H. Tian, C. Jin, P. Strasser and R. Z. Yang, *Adv. Funct. Mater.*, 2020, **30**, 2000503.
78 M. L. Liu, Z. P. Zhao, X. F. Duan and Y. Huang, *Adv. Mater.*, 2019, **31**, 1802234.
79 E. P. George, W. A. Curtin and C. C. Tasan, *Acta Mater.*, 2020, **188**, 435–474.
80 Z. Q. Chen, J. B. Wen, C. H. Wang and X. W. Kang, *Small*, 2022, **18**, 2204255.
81 S. L. A. Bueno, A. Leonardi, N. Kar, K. Chatterjee, X. Zhan, C. Q. Chen, Z. Y. Wang, M. Engel, V. Fung and S. E. Skrabalak, *ACS Nano*, 2022, **16**, 18873–18885.
82 P. Zhang, X. B. Hui, Y. J. Nie, R. T. Wang, C. X. Wang, Z. W. Zhang and L. W. Yin, +.
83 K. Y. Zhu, X. F. Zhu and W. S. Yang, *Angew. Chem., Int. Ed.*, 2019, **58**, 1252–1265.
84 Z. P. Wu, X. F. Lu, S. Q. Zang and X. W. Lou, *Adv. Funct. Mater.*, 2020, **30**, 1910274.
85 W. H. Wang, Y. Yang, D. M. Huan, L. K. Wang, N. Shi, Y. Xie, C. R. Xia, R. R. Peng and Y. L. Lu, *J. Mater. Chem. A*, 2019, **7**, 12538–12546.
86 T. X. Nguyen, Y. C. Liao, C. C. Lin, Y. H. Su and J. M. Ting, *Adv. Funct. Mater.*, 2021, **31**, 2101632.
87 L. He, H. J. Kang, G. Y. Hou, X. S. Qiao, X. Jia, W. Qin and X. H. Wu, *Chem. Eng. J.*, 2023, **460**, 141675.
88 J. J. Yang, C. L. Wang, D. L. Xie, H. Q. Qin, W. J. Liu, M. L. Liang, X. Li, C. Liu and M. Huang, *Surf. Coat. Technol.*, 2023, **457**, 129320.
89 J. Qu, A. Elgendy, R. S. Cai, M. A. Buckingham, A. A. Papaderakis, H. de Latour, K. Hazeldine, G. F. S. Whitehead, F. Alam, C. T. Smith, D. J. Binks, A. Walton, J. M. Skelton, R. A. W. Dryfe, S. J. Haigh and D. J. Lewis, *Adv. Sci.*, 2023, **10**, 2204488.
90 A. Abdelhafiz, B. M. Wang, A. R. Harutyunyan and J. Li, *Adv. Energy Mater.*, 2022, **12**, 2200742.
91 M. J. Cui, C. P. Yang, B. Y. Li, Q. Dong, M. L. Wu, S. Hwang, H. Xie, X. Z. Wang, G. F. Wang and L. B. Hu, *Adv. Energy Mater.*, 2020, **11**, 2002887.
92 M. Han, C. H. Wang, J. Zhong, J. R. Han, N. Wang, A. Seifitokaldani, Y. F. Yu, Y. C. Liu, X. H. Sun, A. Vomiero and H. Y. Liang, *Appl. Catal., B*, 2022, **301**, 120764.
93 N. Li, J. Liu, B. X. Dong and Y. Q. Lan, *Angew. Chem., Int. Ed.*, 2020, **59**, 20779–20793.
94 Z. L. Chen, H. L. Qing, K. Zhou, D. L. Sun and R. B. Wu, *Prog. Mater. Sci.*, 2020, **108**, 100618.
95 Z. X. Cai, H. Goou, Y. Ito, T. Tokunaga, M. Miyauchi, H. Abe and T. Fujita, *Chem. Sci.*, 2021, **12**, 11306–11315.
96 S. Q. Wang, B. L. Xu, W. Y. Huo, H. C. Feng, X. F. Zhou, F. Fang, Z. H. Xie, J. K. Shang and J. Q. Jiang, *Appl. Catal., B*, 2022, **313**, 121472.
97 X. B. Fu, J. H. Zhang, S. Q. Zhan, F. J. Xia, C. J. Wang, D. S. Ma, Q. Yue, J. S. Wu and Y. J. Kang, *ACS Catal.*, 2022, **12**, 11955–11959.
98 J. Kwon, S. Sun, S. Choi, K. Lee, S. Jo, K. Park, Y. K. Kim, H. B. Park, H. Y. Park, J. H. Jang, H. Han, U. Paik and T. Song, *Adv. Mater.*, 2023, **35**, 2300091.
99 Y. Q. Kang, O. Cretu, J. Kikkawa, K. Kimoto, H. Nara, A. S. Nugraha, H. Kawamoto, M. Eguchi, T. Liao, Z. Q. Sun, T. Asahi and Y. Yamauchi, *Nat. Commun.*, 2023, **14**, 4182.
100 N. Han, P. Ding, L. He, Y. Y. Li and Y. G. Li, *Adv. Energy Mater.*, 2020, **10**, 1902338.
101 L. H. Li, Y. Zhang, T. J. Zhou, K. C. Wang, C. Wang, T. Wang, L. W. Yuan, K. X. An, C. H. Zhou and G. N. Lu, *Nat. Commun.*, 2022, **13**, 5315.
102 G. Supran, S. Rahmstorf and N. Oreskes, *Science*, 2023, **379**, eabk0063.
103 X. L. Zhang, X. H. Sun, S. X. Guo, A. M. Bond and J. Zhang, *Energy Environ. Sci.*, 2019, **12**, 1334–1340.
104 J. K. Pedersen, T. A. A. Batchelor, A. Bagger and J. Rossmeisl, *ACS Catal.*, 2020, **10**, 2169–2176.
105 Z. W. Chen, Z. Gariepy, L. X. Chen, X. Yao, A. Anand, S.-J. Liu, C. G. Tetsassi Feugmo, I. Tamblyn and C. V. Singh, *ACS Catal.*, 2022, **12**, 14864–14871.
106 S. Nellaiappan, N. K. Katiyar, R. Kumar, A. Parui, K. D. Malviya, K. G. Pradeep, A. K. Singh, S. Sharma, C. S. Tiwary and K. Biswas, *ACS Catal.*, 2020, **10**, 3658–3663.
107 H. J. Li, H. G. Huang, Y. Chen, F. L. Lai, H. Fu, L. S. Zhang, N. Zhang, S. X. Bai and T. X. Liu, *Adv. Mater.*, 2023, **35**, e2209242.
108 C. Bianchini and P. K. Shen, *Chem. Rev.*, 2009, **109**, 4183–4206.
109 D. S. Wu, K. Kusada, T. Yamamoto, T. Toriyama, S. Matsumura, S. Kawaguchi, Y. Kubota and H. Kitagawa, *J. Am. Chem. Soc.*, 2020, **142**, 13833–13838.
110 S. Y. Li, J. Q. Wang, X. Lin, G. Q. Xie, Y. Huang, X. J. Liu and H. J. Qiu, *Adv. Funct. Mater.*, 2020, **31**, 2007129.

111 D. P. Fan, K. Guo, Y. Zhang, Q. Q. Hao, M. Han and D. D. Xu, *J. Colloid Interface Sci.*, 2022, **625**, 1012–1021.
112 W. Chen, S. P. Luo, M. Z. Sun, X. Y. Wu, Y. S. Zhou, Y. J. Liao, M. Tang, X. K. Fan, B. L. Huang and Z. W. Quan, *Adv. Mater.*, 2022, **34**, 2206276.
113 D. Y. Feng, Y. B. Dong, L. L. Zhang, X. Ge, W. Zhang, S. Dai and Z. A. Qiao, *Angew. Chem., Int. Ed.*, 2020, **59**, 19503–19509.
114 T. Y. Zhang, H. B. Yu, J. L. Shi, X. D. Wang, H. Luo, D. J. Lin, Z. Liu, C. M. Su, Y. C. Wang and L. Q. Liu, *Adv. Sci.*, 2022, **9**, 2103902.
115 T. L. Cocker, V. Jelic, M. Gupta, S. J. Molesky, J. A. J. Burgess, G. D. L. Reyes, L. V. Titova, Y. Y. Tsui, M. R. Freeman and F. A. Hegmann, *Nat. Photonics*, 2013, **7**, 620–625.
116 E. A. Schriber, D. W. Paley, R. Bolotovsky, D. J. Rosenberg, R. G. Sierra, A. Aquila, D. Mendez, F. Poitevin, J. P. Blaschke, A. Bhowmick, R. P. Kelly, M. Hunter, B. Hayes, D. C. Popple, M. Yeung, C. Pareja-Rivera, S. Lisova, K. Tono, M. Sugahara, S. Owada, T. Kuykendall, K. Y. Yao, P. J. Schuck, D. Solis-Ibarra, N. K. Sauter, A. S. Brewster and J. N. Hohman, *Nature*, 2022, **601**, 360–365.
117 R. J. Yang, L. Mei, Y. Y. Fan, Q. Y. Zhang, H. G. Liao, J. Yang, J. Li and Z. Y. Zeng, *Nat. Protoc.*, 2023, **18**, 555–578.